The Alzheimer's gene *SORL1* is a key regulator of endosomal recycling in human neurons

Swati Mishra[1,2*], Allison Knupp[1,2*], Marcell Szabo[1,2], Chizuru Kinoshita[1,2], Dale W. Hailey[1,2], Yuliang Wang[2,3], and Jessica E. Young[1,2,#]

[1]Department of Laboratory Medicine and Pathology

[2]Institute for Stem Cell and Regenerative Medicine

[3]School of Computer Science and Engineering

University of Washington Seattle WA, 98195, USA

[#]Correspondence: jeyoung@uw.edu

[*]Equal Contribution

ABSTRACT

Background Loss of the Sortilin-related receptor 1 (*SORL1*) gene seems to act as a causal event for Alzheimer's disease (AD). Recent studies have established that loss of *SORL1*, as well as mutations in autosomal dominant AD genes *APP* and *PSEN1/2*, pathogenically converge by swelling early endosomes, AD's cytopathological hallmark. Acting together with the retromer trafficking complex, *SORL1* has been shown to regulate the recycling of the amyloid precursor protein (APP) out of the endosome, contributing to endosomal swelling and to APP misprocessing. We hypothesized that *SORL1* plays a broader role in neuronal endosomal recycling and used human induced pluripotent stem cell derived neurons (hiPSC-Ns) to test this hypothesis. We examined endosomal recycling of three transmembrane proteins linked to AD pathophysiology: APP, the BDNF receptor Tropomyosin-related kinase B (TRKB), and the glutamate receptor subunit AMPA1 (GLUA1).

Methods We used isogenic hiPSCs engineered to have *SORL1* depleted or to have enhanced *SORL1* expression. We differentiated neurons from these cell lines and mapped the trafficking of

APP, TRKB and GLUA1 within the endosomal network using confocal microscopy. We also performed cell surface recycling and lysosomal degradation assays to assess the functionality of the endosomal network. Finally, we analyzed alterations in gene expression in *SORL1* depleted neurons using RNA-sequencing.

Results We find that as with APP, endosomal trafficking of GLUA1 and TRKB is impaired by loss of *SORL1*. Conversely, increased *SORL1* expression enhances endosomal recycling for APP and GLUA1. Our unbiased transcriptomic data further support *SORL1*'s role in endosomal recycling. We observe altered expression networks that regulate cell surface trafficking and neurotrophic signaling

Conclusion Collectively, and together with other recent observations, these findings suggest that *SORL1* is a key and broad regulator of retromer-dependent endosomal recycling in neurons, a conclusion that has both pathogenic and therapeutic implications for Alzheimer's disease.

BACKGROUND

Alzheimer's disease (AD) is a progressive neurodegenerative disorder and the most common cause of dementia. The underlying contributors to AD pathology encompass several biological pathways, including endosomal function, amyloid precursor protein (APP) processing, immune function, synaptic function, and lipid metabolism(Karch and Goate, 2015). Among these, endosomal dysfunction in neurons is emerging as a potential causal mechanism(Small and Petsko, 2020). Mutations in the amyloid precursor protein (*APP*) and the two presenilins (*PSEN1* and *PSEN2*) lead to early-onset autosomal dominant AD. When these mutations are modelled in human neurons and other systems they cause endosomal swelling, indicative of traffic jams, a phenotype that is a cytopathological hallmark of AD(Cataldo et al., 2000; Choi et al., 2013; Kwart

53 et al., 2019). Recent genetic studies have identified a fourth gene, the trafficking receptor 'sortilin
54 related receptor 1' (*SORL1*), which, when harboring frame-shift mutations leading to premature
55 stop codons, is described as causal for AD(Holstege et al., 2017; Raghavan et al., 2018;
56 Scheltens et al., 2021). Interestingly, *SORL1* is also linked to the more common, late-onset form
57 of AD(Lambert et al., 2013; Rogaeva et al., 2007b) and its expression is lost in sporadic AD brains
58 (Dodson et al., 2006; Thonberg et al., 2017). When modelled in human neurons, *SORL1* depletion
59 phenocopies *APP* and *PSEN* mutations by causing endosomal swelling(Hung et al., 2021; Knupp
60 et al., 2020).
61
62 The *SORL1* gene codes for the protein SORLA, which functions as part of the retromer trafficking
63 complex (Fjorback et al., 2012; Rogaeva et al., 2007a; Small and Gandy, 2006). Retromer
64 recycles cargo out of the early endosome, either from the endosome to the trans-Golgi network
65 or, with greater importance for neurons, back to the cell surface(Fjorback et al., 2012; Seaman,
66 2012). To date, the best evidence for *SORL1*'s role in retromer-dependent endosomal recycling
67 comes from studies investigating APP trafficking(Fjorback et al., 2012; Schmidt et al., 2007;
68 Willnow and Andersen, 2013). Our previous work demonstrated that *SORL1* depletion retains
69 APP in early endosomes, which may contribute to endosomal swelling by blocking
70 recycling(Knupp et al., 2020).
71
72 Retromer-dependent trafficking in neurons, however, also recycles cargo other than APP. For
73 example, retromer is required for the normal recycling of glutamate receptors, a trafficking event
74 that mediates synaptic plasticity and synaptic health, and this dependency occurs independent of
75 retromer's role in APP recycling(Park et al., 2004; Temkin et al., 2017). Neurotrophin receptors
76 are also trafficked through the endosomal system, in a retromer-dependent manner, and are
77 important for synaptic health(Klinger et al., 2015; Patapoutian and Reichardt, 2001; Rohe et al.,
78 2013).

79 Here we used human induced pluripotent stem cell derived-neurons (hiPSC-Ns) to test the
80 hypothesis that *SORL1* plays a broader role in neuronal endosomal recycling. We use our
81 previously described *SORL1*-depleted hiPSC lines to generate hiPSC-Ns, which model the loss
82 of *SORL1* expression that occurs in AD(Knupp et al., 2020). Furthermore, we used previously
83 established cell lines engineered to overexpress *SORL1* 2-3-fold over wild-type levels(Young et
84 al., 2015) to test the effects of enhanced *SORL1* expression in hiPSC-Ns on these trafficking
85 pathways. Importantly, all cell lines are isogenic. We map the trafficking effects these
86 manipulations have on three specific receptors, APP, the GLUA1 subunit of the AMPA receptor,
87 and neurotrophin receptor TRKB, all of which are implicated in AD (Devi and Ohno, 2015; Dewar
88 et al., 1991; Ginsberg et al., 2019; Martin-Belmonte et al., 2020; Wakabayashi et al., 1999;
89 Yasuda et al., 1995).
90
91 Finally, we performed RNA-sequencing on the *SORL1* depleted cell lines to explore an unbiased
92 transcriptomics analysis induced by *SORL1* depletion. The results generally confirmed our
93 hypothesis, showing that *SORL1* is a key and broad regulator of endosomal recycling in neurons,
94 a conclusion that has both pathogenic and therapeutic implications.
95
96 **RESULTS**
97 ***SORL1* depletion increases neuronal cargo localization in early endosomes.**
98 Using CRISPR/Cas9 genome editing techniques, we previously generated hiPSC-derived
99 neurons (hiPSC-Ns) deficient in *SORL1* expression due to indels introduced in exon 6. We
100 demonstrated that loss of *SORL1* expression in these neurons leads to enlarged early endosomes
101 and an increased colocalization of APP within early endosomes, indicative of endosomal traffic
102 jams(Knupp et al., 2020). We utilized these same cell lines (hereafter referred to as *SORL1*KO
103 and their guide-matched isogenic wild-type clones referred to as WT) to examine localization of
104 the BDNF receptor TRKB and the GLUA1 subunit of the neuronal AMPA receptor. TRKB has

105 been shown to bind to SORLA and this interaction mediates trafficking of TRKB to synaptic
106 plasma membranes(Rohe et al., 2013). GLUA1 is trafficked via the retromer complex, of which
107 SORLA is an adaptor protein(Fjorback et al., 2012; Temkin et al., 2017) and both of these cargo
108 are important in maintaining healthy neuronal function. Because we previously observed an
109 increase in APP localization in early endosomes, resulting in a decrease in localization in
110 downstream vesicles such as Ras-related protein (Rab)7+ late endosomes with *SORL1*
111 depletion(Knupp et al., 2020), we performed an immunocytochemical analysis of both TRKB and
112 GLUA1 localization with the early endosome marker EEA1. Similar to our previous observations
113 for APP, we documented significantly increased localization of both TRKB (Figure 1A) and GLUA1
114 (Figure 1B) in early endosomes in *SORL1*KOneurons as compared to isogenic WT control
115 neurons. Accumulation of neuronal cargo in early endosomes is indicative of endosomal traffic
116 jams, which are thought to impact the transit of cellular cargo through other arms of the endo-
117 lysosomal network.
118
119 ***SORL1* depletion mis-traffics cargo throughout the endo-lysosomal system**
120 The early endosome serves as a hub in which internalized cargo can be retrogradely transported
121 to the trans-Golgi, recycled back to the cell surface or degraded as endosomes mature into late
122 endosomes and lysosomes(Mayle et al., 2012). We have previously observed that APP
123 localization within the trans-Golgi network was decreased in *SORL1*KO neurons(Knupp et al.,
124 2020). Here we tested whether trafficking to the degradative arm of the endo-lysosomal network
125 was affected in our *SORL1*KO neurons. Trafficking of substrates out of the early endosome to
126 late endosomes and, subsequently, lysosomes is important for protein degradation and SORLA
127 has been previously implicated in promoting Aβ degradation via lysosomes(Caglayan et al.,
128 2014). We treated *SORL1* deficient neurons with DQ Red BSA, a proteolysis sensitive fluorogenic
129 substrate that generates fluorescence only when enzymatically cleaved in intracellular lysosomal
130 compartments. Since substrate degradation primarily occurs in lysosomes, altered fluorescence

131 intensity of this reagent is a readout of altered lysosomal degradation(Marwaha and Sharma,
132 2017). We analyzed DQ Red BSA treated neurons for fluorescence intensity using confocal
133 microscopy. Consistent with loss of *SORL1* leading to endosomal traffic jams, we observed a
134 significant reduction of DQ Red BSA fluorescence intensity in *SORL1*KO neurons compared to
135 isogenic WT controls (Figure 2A). We next performed immunocytochemical staining to quantify
136 the colocalization of our selected neuronal cargo with Rab7, a marker of late endosomes, and
137 LAMP1 (Lysosomal Associated Membrane Protein 1), a lysosome marker. We show a significant
138 decrease in co-localization of TRKB (Figure 2B) and GLUA1 (Figure 2C) with Rab7. This result is
139 consistent with our previous observation for APP (Knupp et al., 2020). We analyzed colocalization
140 of these cargo with LAMP1 and we observed a significant decrease with APP (Figure 2D) and
141 TRKB (Figure 2E) and a trend of a decrease with GLUA1 (Figure 2F). These data indicate some
142 fluidity in the network but suggest that trafficking of APP, TRKB and GLUA1 to late
143 endosomes/lysosomes is all decreased by *SORL1*KO, although GLUA1 may be more likely to be
144 trafficked to cell surface pathways or utilizes other adaptor proteins for late endosome to
145 lysosomal trafficking.
146
147 Lysosome size can influence lysosome function and is altered in AD(de Araujo et al., 2020; Hwang
148 et al., 2019). Similarly, location and number of lysosomes within neurons can alter degradative
149 activity (Cheng et al., 2018; Farfel-Becker et al., 2019; Gowrishankar et al., 2015; Yap et al.,
150 2018) and in some cases, altered lysosomal distribution may represent an early neuropathological
151 defect(Zigdon et al., 2017).Recently, loss of *SORL1* in hiPSC neurons was shown to contribute
152 to lysosome dysfunction as indicated by both increased lysosome size and number as well as
153 decreased cathepsin-D activity(Hung et al., 2021). Therefore, we first analyzed LAMP1-
154 immunopositive puncta and also documented a significant increase in lysosome size and number
155 in our *SORL1*KO neurons (Supplemental Figure 1A).
156

157 Next, we analyzed co-localization of Cathepsin-D and LAMP1 to determine if loss of *SORL1*
158 expression leads to altered Cathepsin-D trafficking in neurons. Retromer trafficking is required to
159 deliver one of the most abundant lysosomal proteases, pro-cathepsin D, to lysosomes via the
160 mannose-6-phosphate receptor (M6PR)(Qureshi et al., 2018; Seaman, 2004). The SORLA
161 protein has GGA domains similar to that of M6PR(Spoelgen et al., 2006), and mis-trafficking of
162 Cathepsin-D to lysosomes could affect the maturation and degradative capacity of these
163 organelles. Therefore, we analyzed co-localization of Cathepsin-D and LAMP1 to determine if
164 loss of *SORL1* expression leads to altered Cathepsin-D trafficking in neurons. However, we did
165 not observe a change in Cathepsin-D colocalization between WT and *SORL*1KO (Supplemental
166 Figure 1B). Taken together, our data suggest that *SORL1* loss in neurons reduces trafficking of
167 cargo out of the early endosome to the late endosome and lysosome, contributing to lysosome
168 stress as evidenced by an increase in size and number in these conditions while the decreased
169 cathepsin-D activity observed upon *SORL1* loss(Hung et al., 2021) may not be due to impairment
170 of lysosomal trafficking of the enzyme.
171
172 ***SORL1* depletion targets the endosomal recycling pathway**
173 Another route out of the early endosome is via the endocytic recycling complex (ERC) which can
174 send cargo either to the cell surface or to the trans-Golgi network(Grant and Donaldson, 2009;
175 Mallard et al., 1998; Marsh et al., 1995; Maxfield and McGraw, 2004). To directly examine if
176 *SORL1* expression alters recycling function, we performed a transferrin recycling assay using
177 confocal microscopy. Transferrin can be recycled via a fast pathway within approximately 5-10
178 minutes after being internalized or via a slower pathway involving the ERC over longer periods of
179 time(Ouellette and Carabeo, 2010; Sonnichsen et al., 2000). We examined the fluorescence
180 intensity of Alexa Fluor 647-conjugated transferrin over a 40-minute time course in WT and
181 *SORL1*KO neurons and observed that a higher percentage of intracellular fluorescent transferrin
182 persisted in *SORL1*KO neurons at both early and later time points as compared to WT neurons,

183 indicating reduced recycling pathway function (Figure 3A). Cargo destined for the cell surface can
184 transit to the ERC via Rab11+ recycling endosomes (Ren et al., 1998). Altered size of recycling
185 endosomes can be indicative of dysfunctional recycling of cargo through these compartments.
186 We tested whether loss of *SORL1* expression affected the size of Rab11+ recycling endosomes.
187 Interestingly, we observed a significant increase in the size of Rab11+ recycling endosomes in
188 the *SORL1*KO neurons (Figure 3B), suggesting that this endosomal compartment is also under
189 stress. To test if increased size is due to abnormal cargo trafficking through recycling endosomes,
190 we assessed colocalization of APP, TRKB and GLUA1 with Rab11 and observed increased co-
191 localization of all three cargo with Rab11+ structures in *SORL1*KO neurons compared to WT
192 neurons (Figure 3C-E). Together, these data demonstrate that loss of *SORL1* impacts neuronal
193 recycling endosome pathways by causing traffic jams in the recycling endosomes, similar to the
194 effect that *SORL1* loss has on early endosomes.
195
196 ***SORL1* depletion reduces cell surface levels of cargo.**
197 Together, our data indicate that *SORL1*KO neurons have impaired cargo recycling with increased
198 retention of cargo in recycling endosomes. These observations led us to test whether this cargo
199 was indeed trafficked to the cell surface. A portion of APP has been shown to return to the cell
200 surface via recycling endosomes(Das et al., 2016) and SORLA can interact with the sorting nexin
201 SNX27 to return APP to the cell surface(Das et al., 2016; Huang et al., 2016), although in that
202 study the exact compartment was not described. Furthermore, recycling endosomes are the
203 source for AMPA receptors during long-term potentiation(Park et al., 2004). We therefore
204 examined cell surface levels of APP and GLUA1 using immunofluorescence and confocal
205 microscopy. We documented a significant decrease in cell surface staining of both APP (Figure
206 4A) and GLUA1 (Figure 4B) in *SORL1*KO neurons as compared to WT, consistent with our
207 hypothesis that SORLA is involved in regulating traffic from recycling endosomes.
208

209 ***SORL1* overexpression enhances endosomal recycling**

210 Defects in cell surface recycling have severe consequences in neurons, especially as these
211 processes are necessary for healthy neuronal function. Synapse loss is a main component of AD
212 neurodegeneration and enhancing pathways that support healthy synaptic function may be
213 beneficial. We utilized previously generated cell lines that overexpress *SORL1* cDNA using the
214 piggybac transposon system(Young et al., 2015) to test whether increased *SORL1* expression
215 may enhance the trafficking pathways that are impaired in the *SORL1*KO neurons. Importantly,
216 the *SORL1* overexpressing (*SORL1*OE) cell line and control were generated in the same genetic
217 background as our *SORL1*KO and isogenic WT cell lines. While we found no effect of enhanced
218 *SORL1* expression on DQ Red BSA signal in *SORL1*OE neurons (Supplemental Figure 2A), we
219 did observe increased localization of the three tested cargo (APP, TRKB, and GLUA1) in late
220 endosomes and lysosomes in these cells (Supplemental Figure 2B-D and 2E-G), suggesting that
221 increased *SORL1* expression may enhance cargo trafficking to the degradative pathway.

222

223 We analyzed recycling function using the transferrin recycling assay and observed that *SORL1*OE
224 neurons showed significantly faster transferrin recycling (Figure 5A). We next tested whether
225 colocalization of cargo with recycling endosomes and cell surface recycling was altered between
226 *SORL1*OE and WT neurons. Interestingly, the size of Rab11+ recycling endosomes was
227 significantly smaller in *SORL1*OE neurons (Figure 5B) possibly indicating that increased *SORL1*
228 expression is clearing cargo more rapidly from this compartment. We observed a significant
229 increase in localization of cargo with Rab11+ recycling endosomes (Figure 5C-E). While this result
230 was initially surprising, as we also saw increased colocalization with Rab11+recycling endosomes
231 in our *SORL1*KO neurons (Figure 3C-E), we further documented a significant increase of APP
232 and GLUA1 on the cell surface compared to WT neurons with only endogenous *SORL1*
233 expression (Figure 5F and 5G), as opposed to decreased APP and GLUA1 localization on the
234 cell surface in *SORL1*KO neurons (Figure 4A and 4B). These results suggest that cell surface

235 trafficking via a Rab11 pathway is enhanced by increased *SORL1* expression and that a crucial
236 action of SORLA is the trafficking out of recycling endosomes. Thus, our data support a critical
237 role for SORLA for trafficking cargo from recycling endosomes to the cell surface. In addition, we
238 show for the first time that SORLA levels may regulate cell surface recycling of AMPA receptor
239 subunits in human neurons.
240
241 ***SORL1* depletion's effect on gene expression**.
242 To determine a more global effect of chronic *SORL1* loss in human neurons, we performed bulk
243 RNA sequencing of *SORL1*KO neurons compared to WT neurons. Interestingly, we observed that
244 there were significantly more down-regulated genes in *SORL1*KO neurons than upregulated ones
245 (Supplemental Figure 2B). While none of the cargo we explicitly studied in this work was
246 differentially expressed, GO analysis showed that the top downregulated molecular function
247 pathways in the *SORL1*KO cells were related to receptor-ligand activity and extracellular matrix
248 organization (Figure 6A). The top upregulated molecular function pathways were related to ion
249 channel activity (Figure 6B). To understand these data in the context of an integrated network,
250 we used an analysis method that infers ligand receptor interactions from bulk RNA-seq
251 data(Ramilowski et al., 2015; Wang et al., 2020). We observed several nodes of altered receptor-
252 ligand interactions that indicate altered cell surface recycling and neurotrophic activity (Figure
253 6C). These include alterations in β-integrin signaling, which is consistent with previous work
254 showing reduced β-integrin on the cell surface in *SORL1*KO cancer cells(Pietila et al., 2019), and
255 altered interactions in ephrins/ephrin receptors, also corroborating previous work implicating
256 *SORL1* expression in ephrin signaling and synapse regulation(Huang et al., 2017). Our analysis
257 also showed nodes with alterations in nerve growth factor/nerve growth factor receptor
258 (NGF/NGFR) and fibroblast growth factor/fibroblast growth factor receptor (FGF/FGFR) signaling,
259 indicating alterations in neurotrophin and growth factor signaling and suggesting that the presence

260 of endosomal traffic jams in *SORL1*KO neurons may ultimately impact multiple pathways
261 important for neuronal health and development.

262 **DISCUSSION**

263 Trafficking through the endo-lysosomal network regulates intra-cellular location of proteins,
264 dictating their homeostasis, function and influence on cellular physiology. Functional studies by
265 our group and others document endosomal abnormalities in hiPSC-derived neuronal models of
266 AD(Hung et al., 2021; Knupp et al., 2020; Kwart et al., 2019). Emerging from this evidence is the
267 role of *SORL1* as an endosomal gene that plays essential roles in mediating cargo trafficking.
268 Recent work has implicated *SORL1* as AD's fourth causal gene(Olav M. Andersen, 2021;
269 Scheltens et al., 2021), and of these genes it is the only one linked to the common late-onset form
270 of the disease. Understanding *SORL1*'s function is paramount for understanding AD's pathogenic
271 mechanisms and for potential therapeutic interventions.

272

273 Acting as a receptor of the retromer trafficking complex, SORLA has already been pathogenically
274 linked to AD by its role in recycling APP out of endosomes(Andersen et al., 2005; Herskowitz et
275 al., 2012; Offe et al., 2006). This current work and our previous study(Knupp et al., 2020) shows
276 that *SORL1* depletion leads to increased APP localization in early and recycling endosomes. By
277 lengthening the residence time of APP in these endosomal compartments, accelerated
278 amyloidogenic cleavage of APP occurs due to the close proximity of APP and BACE1(Sun and
279 Roy, 2018). Indeed, loss of *SORL1* leads to the accumulation of Aβ peptides, an antecedent of
280 'amyloid pathology' (Andersen et al., 2005; Knupp et al., 2020; Rogaeva et al., 2007b). We
281 hypothesized that loss of *SORL1* in neurons would impact other cargo important for healthy
282 neuronal function. To test this hypothesis, in addition to APP, we examined localization of the
283 neurotrophin receptor TRKB and the GLUA1 subunit of the AMPA receptor. These cargo link to
284 another key pathology of AD: neurodegeneration, a slowly progressive process that begins with

synaptic dysfunction characterized by glutamate receptor loss, which then progresses to synaptic loss before ultimately, over years, leading to widespread neuronal cell death (Selkoe, 2002).

Our experiments point to *SORL1*'s key role in cell surface recycling. By using a prototypical cargo, transferrin, we demonstrate a reciprocal role between loss and enhancement of *SORL1* expression in cell surface recycling. Specifically, by showing that *SORL1* plays a role in recycling glutamate receptors, a trafficking event critical for preventing synaptic dysfunction and synaptic loss, our results link *SORL1* to AD's early-stage neurodegenerative process. Since retromer-dependent glutamate receptor recycling has been shown to occur independent of APP(Temkin et al., 2017), our results suggest that *SORL1* mutations can, at least in principle, drive two key AD pathologies, amyloid pathology and synaptic pathology, through parallel mechanisms(Small and Petsko, 2020).

Interestingly, AD's defining cytopathology, swollen endosomes, also seems to occur independent of Aβ peptides. In the case of early-onset causal genes, studies have shown that APP and PSEN mutations lead to endosomal swelling even when the production of Aβ peptides are arrested, but is driven instead by an APP intermediate, the β–C-terminal fragment produced by BACE1 cleavage(Kwart et al., 2019). We previously demonstrated that endosomal swelling occurs in *SORL1*KO neurons even when BACE1 is inhibited(Knupp et al., 2020). However, a recent study showed that there is a reduction in endosomal swelling when total APP expression is reduced(Hung et al., 2021). One interpretation that reconciles these findings is that reduction of cargo in general, especially one as abundant as APP, may relieve some of the stress on neuronal endosomes induced by *SORL1* deficiency. Collectively, however, our data suggest that AD's core histopathology, amyloid plaques, and cytopathology, swollen endosomes, occur through parallel events.

310 To test the hypothesis that *SORL1* functions more broadly in neuronal endosomal recycling, we
311 measured recycling endosome size and showed that, in addition to APP and GLUA1, the
312 neurotrophin receptor TRKB, is dependent on *SORL1* for normal endosomal trafficking. TRKB is
313 part of a different family of proteins that depend on retromer-dependent endosomal recycling for
314 its normal trafficking, and one that has been linked to synaptic health(Klinger et al., 2015; Rohe
315 et al., 2013) (Patapoutian and Reichardt, 2001).
316
317 Our unbiased transcriptomic screen further supported that neurotrophic signaling and cell surface
318 recycling pathways are impacted by *SORL1* deficiency. Our goal for this analysis was to
319 determine the global effect of *SORL1* loss on neuronal networks. Indeed, our analysis does not
320 show that the specific cargo proteins described here are differentially expressed. However, the
321 analysis does indicate that loss of *SORL1* in human neurons impacts cell surface networks,
322 including receptor ligand interactions in neurotrophic and growth factor pathways, β-integrin
323 signaling, and ephrin signaling. Our analysis corroborates previous work and the altered networks
324 we observe impact neuronal health, axonal guidance, and synapse formation(Huang et al., 2017;
325 Huang et al., 2006; Pietila et al., 2019).
326
327 The early endosome is considered the central station in the sorting and trafficking of cargo
328 throughout the many stations of the endo-lysosomal system. While the early endosome is the
329 station that is affected first and foremost in AD, it is not surprising that a primary dysfunction in
330 this central station will secondarily influence trafficking throughout the system. Our work, along
331 with other recent work(Hung et al., 2021) also supports a role for *SORL1* in lysosomal trafficking
332 in neurons. We observed an increase in lysosome size and altered localization of APP, TRKB,
333 and GLUA1 in late endosomes and lysosomes in *SORL1*KO neurons. Hung et al., also reported
334 decreased Cathepsin-D activity in *SORL1* deficient neurons, suggesting that *SORL1* loss directly
335 impacts lysosome function. We interpret our functional and colocalization data to suggest that

336 loss of *SORL1* expression mainly affects trafficking of cargo to lysosomes, but our data does not
337 rule out a role of SORLA in neuronal lysosome function. While we did not observe a difference
338 in Cathepsin-D localization to lysosomes, it is important to note that that LAMP1 only partially
339 colocalizes with Cathepsin-D in neurons (Cheng et al., 2018). Furthermore, the loss of proteolytic
340 activity evidenced by decreased intensity of DQ Red BSA in *SORL1*KO neurons may not be
341 completely due to reduced trafficking to lysosomes but could be a result of abnormal lysosomal
342 function as DQ Red BSA is internalized by a process called macropinocytosis wherein
343 macropinosomes can be directly trafficked to lysosomes (Hamasaki et al., 2004; Lorenzen et al.,
344 2010; Racoosin and Swanson, 1993). Thus, the loss of proteolytic activity evidenced by
345 decreased intensity of DQ Red BSA in *SORL1*KO neurons may not be completely due to reduced
346 trafficking to lysosomes but could also be a result of abnormal lysosomal function.

347 **CONCLUSION**

348 While the secondary downstream effects induced by *SORL1* depletion in the endo-lysosomal
349 system are interesting and likely relevant to AD's ultimate pathogenesis, from a therapeutic
350 perspective it is best to target *SORL1*'s primary defect, which seems to localize to the endosomal
351 recycling pathway. Interestingly, recent biomarker studies suggest that defects in retromer-
352 dependent endosomal recycling occur in a majority of patients with 'sporadic' AD(Simoes et al.,
353 2020), suggesting that the observed *SORL1*-induced defects may generalize across early and
354 late onset forms of the disorder. Collectively, our results support the conclusion that *SORL1*, and
355 the retromer-dependent pathway in which it functions, is a valid therapeutic target and
356 interventions directed at this pathway may ameliorate endosomal recycling defects that seem to
357 act as, at least, one primary driver of AD.

358

359 **METHODS**

360 **Cell lines**

361 ***Cell lines generated by CRIPSR/Cas9 gene editing technology***

362 The generation of the cell lines used in this paper is described in our previously published work
363 (Knupp et al., 2020) and consists of four clones: Two wild-type clones, designated clone A6 and
364 clone A7, and two *SORL1*KO clones, designated clone E1 and clone E4. Cell lines were
365 generated from our previously published and characterized CV background human induced
366 pluripotent stem cell line(Young et al., 2015). This cell line is male and has a APOE ε3/ε4
367 genotype(Levy et al., 2007). All four clones were shown to have normal karyotypes and are
368 routinely tested for mycoplasma (MycoAlert).
369
370 **CRISPR/Cas9 gRNA, ssODN, and Primer Sequences** gRNA: ATTGAACGACATGAACCCTC
371 ssODN:
372 GGGAATTGATCCCTATGACAAACCAAATACCATCTACATTGAACGACATGAACCCTCTGGC
373 TACTCCACGTCTTCCGA AGTACAGATTTCTTCCAGTCCCGGGAAAACCAGGAAG Forward
374 primer: ctctatcctgagtcaaggagtaac Reverse primer: ccttccaattcctgtgtatgc PCR amplifies 458 bp
375 sequence. These sequences have been previously published in (Knupp et al., 2020)
376
377 ***SORL1 overexpression cell lines*** Isogenic cell lines with overexpression of SORL1 were
378 generated as previously described(Young et al., 2015). These lines are generated from the CV
379 parental line, the same parental line as the *SORL1*KO cell lines were made from. Briefly, stable
380 integration of SORL1 cDNA into the genome was achieved by using piggybac transposon system
381 (Systems Biosciences). Vector alone (WT) or vector with SORL1 cDNA (*SORL1*OE) constructs
382 were introduced into iPSCs by electroporation and stable cell lines were selected with puromycin
383 (2ug/ml) treatment. For all overexpression experiments *SORL1*OE cells were compared to the
384 vector alone controls.
385
386 **hiPSC Neuronal Differentiation**

387 hiPSCs were differentiated to neurons using dual-SMAD inhibition(Chambers et al., 2009; Shi et
388 al., 2012). Briefly, hiPSCs were plated on Matrigel coated 6-well plates at a density of 3.5 million
389 cells per well and fed with Basal Neural Maintenance Media (1:1 DMEM/F12 + glutamine
390 media/neurobasal media, 0.5% N2 supplement, 1% B27 supplement, 0.5% GlutaMax, 0.5%
391 insulin-transferrin-selenium, 0.5% NEAA, 0.2% β-mercaptoethanol; Gibco, Waltham, MA) +
392 10mM SB-431542 + 0.5mM LDN-193189 (Biogems, Westlake Village, CA). Cells were fed daily
393 for seven days. On day eight, cells were incubated with Versene, gently dissociated using cell
394 scrapers, and passaged at a ratio of 1:3. On day nine, media was switched to Basal Neural
395 Maintenance Media and fed daily. On day 13, media was switched to Basal Neural Maintenance
396 Media with 20 ng/mL FGF (R&D Systems, Minneapolis, MN) and fed daily. On day sixteen, cells
397 were passaged again at a ratio of 1:3. Cells were fed until approximately day twenty-three. At this
398 time, cells were FACS sorted to obtain the CD184/CD24 positive, CD44/CD271 negative neural
399 precursor cell (NPC) population. Following sorting, NPCs were expanded for neural
400 differentiation. For cortical neuronal differentiation, NPCs were plated out in 10cm cell culture
401 dishes at a density of 6 million cells/10cm plate. After 24 hours, cells were switched to Neural
402 Differentiation media (DMEM-F12 + glutamine, 0.5% N2 supplement, 1% B27 supplement, 0.5%
403 GlutaMax) + 0.02ug/mL brain-derived neurotrophic factor (PeproTech, Rocky Hill, NJ) +
404 0.02ug/mL glial-cell-derived neurotrophic factor (PeproTech) + 0.5mM dbcAMP (Sigma Aldrich,
405 St Louis, MO). Media was refreshed twice a week for three weeks. After three weeks, neurons
406 were selected for CD184/CD44/CD271 negative population by MACS sorting and plated for
407 experiments.
408
409 **Purification of Neurons**
410 Following three weeks of differentiation, neurons were dissociated with accutase and
411 resuspended in Magnet Activated Cell Sorting (MACS) buffer (PBS + 0.5% bovine serum albumin
412 [Sigma Aldrich, St Louis, MO] + 2mM ethylenediaminetetraacetic acid [Thermo Fisher Scientific,

413 Waltham, MA]). Following a modification of (Yuan et al., 2011), cells were incubated with PE-
414 conjugated mouse anti-Human CD44 and mouse anti-Human CD184 antibodies (BD
415 Biosciences, San Jose, CA) at a concentration of 5µl/10 million cells. Following antibody
416 incubation, cells were washed with MACS buffer and incubated with anti-PE magnetic beads (BD
417 Biosciences, San Jose, CA) at a concentration of 25µl/10 million cells. Bead-antibody complexes
418 were pulled down using a rare earth magnet, supernatants were selected, washed, and plated at
419 an appropriate density.
420
421 **DQ Red BSA assay for visualization of lysosomal degradation**
422 Lysosomal proteolytic degradation was evaluated using DQ Red BSA (#D-12051; Thermo Fisher
423 Scientific), a fluorogenic substrate for lysosomal proteases, that generates fluorescence only
424 when enzymatically cleaved in intracellular lysosomal compartments. hiPSC-derived neurons
425 were seeded at a density of 400,000 cells/well of a matrigel coated 48 well plate. After 24 hours,
426 cells were washed once with DPBS, treated with complete media containing either 10µg/ml DQ
427 Red BSA or vehicle (PBS) and incubated for 5 hours at 37°C in a 5% CO_2 incubator as described
428 in(Marwaha and Sharma, 2017). At the end of 5 hours, cells were washed with PBS, fixed with
429 4% PFA and immunocytochemistry was performed as described in methods. Cells were imaged
430 using a Leica SP8 confocal microscope and all image processing was completed with ImageJ
431 software. Cell bodies were identified by MAP2 labeling, and fluorescence intensity of DQ Red
432 BSA was measured in regions of the images containing the MAP2 label.
433
434 **Immunocytochemistry**
435 For immunocytochemistry, cells were fixed with 4% PFA for 20 minutes. Fixed cells were washed
436 three times with PBST (PBS with 0.05% tween 20), permeabilized with Triton X-100 in PBS for
437 15 minutes, washed twice again with PBST, blocked with 5% BSA in PBS at room temperature
438 for 1h and incubated with appropriate primary antibodies overnight at 4°C. The next day, cells

439 were incubated with appropriate secondary antibodies and 1µg/ml DAPI for 1 hour at RT, washed
440 three times with PBST and mounted on glass slides with Prolong Gold Antifade mountant
441 (#P36930; Thermo Fisher Scientific).
442
443 **Colocalization analysis**
444 To investigate colocalization with endo-lysosomal compartments, hiPSC-derived neurons were
445 labeled with markers specific for each intra-cellular compartment (EEA1 for early endosomes,
446 Rab7 for late endosomes, LAMP1 for lysosomes and Rab11 for recycling endosomes) using
447 immunocytochemistry. A minimum of 10 fields of confocal z-stack images were captured under
448 blinded conditions using a Yokogawa W1 spinning disk confocal microscope (Nikon) and a 100X
449 plan apochromat oil immersion objective. Median filtering was used to remove noise from images
450 and Otsu thresholding was applied to all images. Colocalization was quantified using the JACOP
451 plugin(Bolte and Cordelieres, 2006) in Image J software(Schindelin et al., 2012) and presented
452 as Mander's correlation coefficient.(Dunn et al., 2011; Manders et al., 1993)
453
454 **Cell Surface Staining:** Cell surface expression of GLUA1 and APP was determined using
455 immunocytochemistry and confocal microscopy. To label proteins at the cell surface, cells were
456 fixed with 4% PFA, washed and treated with primary and secondary antibodies as described in
457 the 'immunocytochemistry' section of methods. Permeabilization with 0.1% Triton X-100 was not
458 performed for this experiment. To label total protein levels, cells were fixed with 4% PFA, washed,
459 permeabilized with 0.1% Triton X-100 and treated with primary and secondary antibodies as
460 described in the 'immunocytochemistry' section of methods. Analysis of fluorescence intensity
461 was done using Image J software. Cell surface expression was represented as ratio of
462 fluorescence intensity measured under non-permeabilized conditions and fluorescence intensity
463 measured under permeabilized conditions.
464

465 **Antibodies**

466 The following primary antibodies were used: Early endosome antigen 1 (EEA1) at 1:500
467 (#610456; BD Biosciences); amyloid precursor protein (APP) at 1:500 (#ab32136; Abcam);
468 microtubule-associated protein 2 (MAP2) at 1:1000 (ab92434; Abcam); Ras-related protein Rab-
469 7a (Rab7) at 1:1000 (ab50533; Abcam); Ras-related protein Rab-11 (Rab11) at 1:250 (#610656;
470 BD Biosciences); Lysosome associated membrane protein-1 (LAMP1) at 1:250 (#sc 2011; Santa
471 Cruz); Tropomyosin receptor kinase B (TRKB; # ab18987; abcam) and GLUA1(# MAB2263;
472 Millipore sigma) at 1:500(DAPI at 1 mg/mL final (Alfa Aesar).

473

474 **Transferrin recycling assay**

475 To measure recycling pathway function, we utilized transferrin recycling assay as previously
476 described(Rapaport et al., 2010). Purified neurons were seeded at 400,000 cells/well of a 24 well
477 plate containing matrigel coated 12 mm glass coverslip/well. After 5 DIV, cells were washed once
478 with DMEM-F12 medium and incubated with starving medium (DMEM-F12 medium+25mM
479 HEPES+ 0.5% BSA) for 30 minutes at 37°C in a 5% CO_2 incubator to remove any residual
480 transferrin. Thereafter, cells were pulsed with either 100µg/ml transferrin from human serum
481 conjugated with Alexa Fluor™ 647(#T23366; Thermo Fisher Scientific) or vehicle (PBS) in
482 'starving medium'. At the end of 10 mins, cells were washed twice with ice-cold PBS to remove
483 any external transferrin and stop internalization of transferrin and washed once with acid stripping
484 buffer (25mM citric acid+24.5mM sodium citrate+280mM sucrose+0.01mM Deferoxamine) to
485 remove any membrane bound transferrin. Next, cells were either fixed in 4% PFA or 'Chase
486 medium' (DMEM-F12+50µM Deferoxamine+20mM HEPES+500µg/ml Holo-transferrin) was
487 added for different time points. Immunocytochemistry was done using MAP2 antibody to label
488 neurons, confocal images were captured using Leica SP8 confocal microscope under blinded
489 conditions. Fluorescence intensity of transferrin was measured using ImageJ software. Recycling

490 function was presented as transferrin fluorescence intensity as a percentage of the fluorescence
491 intensity measured at time zero.

492 **Measurement of lysosome and recycling endosome size**

493 Immunocytochemistry using antibodies for LAMP1 and MAP2 or RAB11 and MAP2 was
494 performed as described above. Using a Leica SP8 confocal microscope with an apochromatic
495 63X oil immersion lens, z-stack images were obtained under blinded conditions. For the LAMP1
496 analysis, 17-34 fields were analyzed for a total of **45 – 76** cells analyzed. For the RAB11 analysis,
497 15-30 fields were analyzed for a total of **59 – 124** cells analyzed. Vesicle size measurements were
498 performed using Cell Profiler software as previously described (Knupp et al., 2020) (McQuin et
499 al., 2018). Briefly, the vesicle channel was masked using the MAP2 channel and automated
500 segmentation algorithms were used to identify individual puncta. The pixel area of each puncta
501 was measured and is presented as mean area of all puncta per field.

502

503 **Statistical Analysis**

504 For all the experiments, at least two independent clones of each genotype were used. For all
505 imaging experiments the data was analyzed in a blinded manner. Experimental data was tested
506 for normal distributions using the ShapiroWilk normality test. Normally distributed data was
507 analyzed using parametric two-tailed unpaired t tests. Non-normally distributed data was analyzed
508 by non-parametric Mann-Whitney test. Significance was defined as a value of $p > 0.05$. All
509 statistical analysis was completed using GraphPad Prism software. Statistical details of individual
510 experiments, including biological and technical replicate information, can be found in the figure
511 legends.

512

513 **RNA- sequencing analysis**

514 *RNA Extraction*

515 RNA was collected from 3 separate differentiations including a combination of two WT clones and
516 two *SORL1*KO clones. Each sample includes 2-3 technical replicates. RNA was collected from 2
517 million purified neurons for each sample. Purification of total RNA was completed using the
518 PureLink RNA Mini Kit (Thermo Fisher 12183018A). Assessment of purified RNA was completed
519 using a NanoDrop. Final RNA quantification was completed using the Quant-iT RNA assay
520 (Invitrogen) and RNA integrity analysis was completed using a fragment analyzer (Advanced
521 Analytical).
522
523 *Library Prep and Sequencing*
524 Library preparation was completed using the TruSeq Stranded mRNA kit (Illumina RS-122-2103)
525 per manufacturer instructions. Sequencing was performed on a NovaSeq 6000 instrument.
526
527 *Data analysis*
528 Raw reads were aligned to GRCh38 with reference transcriptome GENCODE release 29 using
529 STAR v2.6.1d (Dobin, Alexander et al. "STAR: ultrafast universal RNA-seq
530 aligner." *Bioinformatics (Oxford, England)* vol. 29,1 (2013): 15-21.
531 doi:10.1093/bioinformatics/bts635). Gene-level expression quantification is generated by RSEM
532 v1.3.1(Li and Dewey, 2011). Genes with fewer than 20 normalized reads across all samples were
533 omitted from further analysis. We did observe variation in the transcriptome based on
534 differentiation (Supplemental Figure 3A), however this was corrected for using the sva
535 package(Leek et al., 2012).
536
537 To identify differentially expressed genes (DEGs), we used DESeq (Simon Anders and Wolfgang
538 Huber (2010): Briefly, we fit two models: a null model where gene expression only depends on
539 batch effects (i.e., differentiation), and an alternative model where gene expression depends on
540 both genotype (*SORL1*KO vs. WT) and batch effects. Chi-squared tests were performed to

541 compare both fits, and we declare a gene as differentially expressed only when the alternative
542 model fits the expression data better. DEGs are defined as genes with false discovery rate less
543 than 0.05 and fold change greater than 1.5. The top gene ontology (GO) package (Alexa A,
544 Rahnenfuhrer J (2021). *topGO: Enrichment Analysis for Gene Ontology*. R package version
545 2.44.0) was used to identify GO terms that were enriched. GO terms were tested according to the
546 Fisher's exact test. Finally, we mapped DEGs onto receptor-ligand interaction diagrams
547 generated by Ramilowski et al(Ramilowski et al., 2015) using the igraph plugin (Csardi G, Nepusz
548 T (2006). "The igraph software package for complex network research." *InterJournal*, **Complex**
549 **Systems**, 1695. https://igraph.org). To compare the amount of down-regulated vs. up-regulated
550 genes we used a 2-sample test for equality of proportions with continuity correction in R.

551 **Declarations**

552 **Availability of Data and Material**

553 All raw and processed RNA-seq data has been deposited at the NCBI Gene Expression Omnibus
554 (GSE180793). The data sets used and/or analyzed during the current study are available from
555 the corresponding author on reasonable request.

556

557 The authors declare no competing interests

558

559 **Acknowledgements:**

560 We thank Dr. Harald Frankowski, Dr. Yoshito Kinoshita, Ms. Shannon Rose, Ms. Eden
561 Cruickshank and all members of the Young Laboratory for critical discussions and feedback
562 during the preparation of this manuscript. We also thank Dr. Scott A. Small and Dr. Gregory A.
563 Petsko for critical comments, discussions and feedback on this work. We would like to
564 acknowledge the UW SLU Cell Analysis Facility and the Garvey Imaging Core at the UW Institute
565 for Stem Cell and Regenerative Medicine. This work was supported by a NIH grant
566 (R01AG062148) and a BrightFocus Foundation grant (A2018656S) to J.E.Y., a Biogen

567 Sponsored Research Agreement to J.E.Y., a Retromer Therapeutic Sponsored Research
568 Agreement to J.E.Y. and NIH traning grant (T32AG052354) to A.K. and a generous gift from the
569 Ellison Foundation (to UW).

570

571 **Author Contributions:**

572 Conceptualization: J.E.Y., S.M, A.K. Microscopy analysis: S.M, A.K., and D.W.H. RNA-seq
573 analysis and bioinformatics: Y.W and A.K. Methodology: S.M., A.K., M.S., C.K. Writing-Original
574 Draft: S.M., A.K. and J.E.Y. Writing-Reviewing and editing: J.E.Y., S.M., A.K. Funding Acquisition:
575 J.E.Y. and A.K. Supervision: J.E.Y.

576

577

578

579

580 **References**

581 Andersen, O.M., Reiche, J., Schmidt, V., Gotthardt, M., Spoelgen, R., Behlke, J., von Arnim, C.A.,
582 Breiderhoff, T., Jansen, P., Wu, X*., et al.* (2005). Neuronal sorting protein-related receptor
583 sorLA/LR11 regulates processing of the amyloid precursor protein. Proc Natl Acad Sci U S A *102*,
584 13461-13466.
585 Bolte, S., and Cordelieres, F.P. (2006). A guided tour into subcellular colocalization analysis in light
586 microscopy. J Microsc *224*, 213-232.
587 Caglayan, S., Takagi-Niidome, S., Liao, F., Carlo, A.S., Schmidt, V., Burgert, T., Kitago, Y.,
588 Fuchtbauer, E.M., Fuchtbauer, A., Holtzman, D.M*., et al.* (2014). Lysosomal sorting of amyloid-
589 beta by the SORLA receptor is impaired by a familial Alzheimer's disease mutation. Science
590 translational medicine *6*, 223ra220.
591 Cataldo, A.M., Peterhoff, C.M., Troncoso, J.C., Gomez-Isla, T., Hyman, B.T., and Nixon, R.A. (2000).
592 Endocytic pathway abnormalities precede amyloid beta deposition in sporadic Alzheimer's
593 disease and Down syndrome: differential effects of APOE genotype and presenilin mutations. Am
594 J Pathol *157*, 277-286.
595 Chambers, S.M., Fasano, C.A., Papapetrou, E.P., Tomishima, M., Sadelain, M., and Studer, L.
596 (2009). Highly efficient neural conversion of human ES and iPS cells by dual inhibition of SMAD
597 signaling. Nat Biotechnol *27*, 275-280.
598 Cheng, X.-T., Xie, Y.-X., Zhou, B., Huang, N., Farfel-Becker, T., and Sheng, Z.-H. (2018).
599 Characterization of LAMP1-labeled nondegradative lysosomal and endocytic compartments in
600 neurons. J Cell Biol *217*, 3127-3139.

601 Choi, J.H., Kaur, G., Mazzella, M.J., Morales-Corraliza, J., Levy, E., and Mathews, P.M. (2013). Early
602 endosomal abnormalities and cholinergic neuron degeneration in amyloid-beta protein
603 precursor transgenic mice. J Alzheimers Dis *34*, 691-700.
604 Das, U., Wang, L., Ganguly, A., Saikia, J.M., Wagner, S.L., Koo, E.H., and Roy, S. (2016). Visualizing
605 APP and BACE-1 approximation in neurons yields insight into the amyloidogenic pathway. Nat
606 Neurosci *19*, 55-64.
607 de Araujo, M.E.G., Liebscher, G., Hess, M.W., and Huber, L.A. (2020). Lysosomal size matters.
608 Traffic *21*, 60-75.
609 Devi, L., and Ohno, M. (2015). TrkB reduction exacerbates Alzheimer's disease-like signaling
610 aberrations and memory deficits without affecting β-amyloidosis in 5XFAD mice. Translational
611 psychiatry *5*, e562-e562.
612 Dewar, D., Chalmers, D.T., Graham, D.I., and McCulloch, J. (1991). Glutamate metabotropic and
613 AMPA binding sites are reduced in Alzheimer's disease: an autoradiographic study of the
614 hippocampus. Brain Res *553*, 58-64.
615 Dodson, S.E., Gearing, M., Lippa, C.F., Montine, T.J., Levey, A.I., and Lah, J.J. (2006). LR11/SorLA
616 expression is reduced in sporadic Alzheimer disease but not in familial Alzheimer disease. J
617 Neuropathol Exp Neurol *65*, 866-872.
618 Dunn, K.W., Kamocka, M.M., and McDonald, J.H. (2011). A practical guide to evaluating
619 colocalization in biological microscopy. Am J Physiol Cell Physiol *300*, C723-C742.
620 Farfel-Becker, T., Roney, J.C., Cheng, X.T., Li, S., Cuddy, S.R., and Sheng, Z.H. (2019). Neuronal
621 Soma-Derived Degradative Lysosomes Are Continuously Delivered to Distal Axons to Maintain
622 Local Degradation Capacity. Cell Rep *28*, 51-64.e54.
623 Fjorback, A.W., Seaman, M., Gustafsen, C., Mehmedbasic, A., Gokool, S., Wu, C., Militz, D.,
624 Schmidt, V., Madsen, P., Nyengaard, J.R.*, et al.* (2012). Retromer binds the FANSHY sorting motif
625 in SorLA to regulate amyloid precursor protein sorting and processing. The Journal of
626 neuroscience : the official journal of the Society for Neuroscience *32*, 1467-1480.
627 Ginsberg, S.D., Malek-Ahmadi, M.H., Alldred, M.J., Chen, Y., Chen, K., Chao, M.V., Counts, S.E.,
628 and Mufson, E.J. (2019). Brain-derived neurotrophic factor (BDNF) and TrkB hippocampal gene
629 expression are putative predictors of neuritic plaque and neurofibrillary tangle pathology.
630 Neurobiology of Disease *132*, 104540.
631 Gowrishankar, S., Yuan, P., Wu, Y., Schrag, M., Paradise, S., Grutzendler, J., De Camilli, P., and
632 Ferguson, S.M. (2015). Massive accumulation of luminal protease-deficient axonal lysosomes at
633 Alzheimer's disease amyloid plaques. Proceedings of the National Academy of Sciences *112*,
634 E3699-E3708.
635 Grant, B.D., and Donaldson, J.G. (2009). Pathways and mechanisms of endocytic recycling. Nat
636 Rev Mol Cell Biol *10*, 597-608.
637 Hamasaki, M., Araki, N., and Hatae, T. (2004). Association of early endosomal autoantigen 1 with
638 macropinocytosis in EGF-stimulated A431 cells. Anat Rec A Discov Mol Cell Evol Biol *277*, 298-
639 306.
640 Herskowitz, J.H., Offe, K., Deshpande, A., Kahn, R.A., Levey, A.I., and Lah, J.J. (2012). GGA1-
641 mediated endocytic traffic of LR11/SorLA alters APP intracellular distribution and amyloid-beta
642 production. Mol Biol Cell *23*, 2645-2657.
643 Holstege, H., van der Lee, S.J., Hulsman, M., Wong, T.H., van Rooij, J.G., Weiss, M.,
644 Louwersheimer, E., Wolters, F.J., Amin, N., Uitterlinden, A.G.*, et al.* (2017). Characterization of

645 pathogenic SORL1 genetic variants for association with Alzheimer's disease: a clinical
646 interpretation strategy. Eur J Hum Genet *25*, 973-981.
647 Huang, T.Y., Zhao, Y., Jiang, L.L., Li, X., Liu, Y., Sun, Y., Pina-Crespo, J.C., Zhu, B., Masliah, E.,
648 Willnow, T.E.*, et al.* (2017). SORLA attenuates EphA4 signaling and amyloid beta-induced
649 neurodegeneration. J Exp Med *214*, 3669-3685.
650 Huang, T.Y., Zhao, Y., Li, X., Wang, X., Tseng, I.C., Thompson, R., Tu, S., Willnow, T.E., Zhang, Y.W.,
651 and Xu, H. (2016). SNX27 and SORLA Interact to Reduce Amyloidogenic Subcellular Distribution
652 and Processing of Amyloid Precursor Protein. The Journal of neuroscience : the official journal of
653 the Society for Neuroscience *36*, 7996-8011.
654 Huang, Z., Shimazu, K., Woo, N.H., Zang, K., Muller, U., Lu, B., and Reichardt, L.F. (2006). Distinct
655 roles of the beta 1-class integrins at the developing and the mature hippocampal excitatory
656 synapse. The Journal of neuroscience : the official journal of the Society for Neuroscience *26*,
657 11208-11219.
658 Hung, C., Tuck, E., Stubbs, V., van der Lee, S.J., Aalfs, C., van Spaendonk, R., Scheltens, P., Hardy,
659 J., Holstege, H., and Livesey, F.J. (2021). SORL1 deficiency in human excitatory neurons causes
660 APP-dependent defects in the endolysosome-autophagy network. Cell Rep *35*, 109259.
661 Hwang, J., Estick, C.M., Ikonne, U.S., Butler, D., Pait, M.C., Elliott, L.H., Ruiz, S., Smith, K.,
662 Rentschler, K.M., Mundell, C.*, et al.* (2019). The Role of Lysosomes in a Broad Disease-Modifying
663 Approach Evaluated across Transgenic Mouse Models of Alzheimer's Disease and Parkinson's
664 Disease and Models of Mild Cognitive Impairment. Int J Mol Sci *20*.
665 Karch, C.M., and Goate, A.M. (2015). Alzheimer's disease risk genes and mechanisms of disease
666 pathogenesis. Biol Psychiatry *77*, 43-51.
667 Klinger, S.C., Siupka, P., and Nielsen, M.S. (2015). Retromer-Mediated Trafficking of
668 Transmembrane Receptors and Transporters. Membranes (Basel) *5*, 288-306.
669 Knupp, A., Mishra, S., Martinez, R., Braggin, J.E., Szabo, M., Kinoshita, C., Hailey, D.W., Small, S.A.,
670 Jayadev, S., and Young, J.E. (2020). Depletion of the AD Risk Gene SORL1 Selectively Impairs
671 Neuronal Endosomal Traffic Independent of Amyloidogenic APP Processing. Cell Rep *31*, 107719.
672 Kwart, D., Gregg, A., Scheckel, C., Murphy, E.A., Paquet, D., Duffield, M., Fak, J., Olsen, O., Darnell,
673 R.B., and Tessier-Lavigne, M. (2019). A Large Panel of Isogenic APP and PSEN1 Mutant Human
674 iPSC Neurons Reveals Shared Endosomal Abnormalities Mediated by APP beta-CTFs, Not Abeta.
675 Neuron *104*, 256-270 e255.
676 Lambert, J.C., Ibrahim-Verbaas, C.A., Harold, D., Naj, A.C., Sims, R., Bellenguez, C., Jun, G.,
677 Destefano, A.L., Bis, J.C., Beecham, G.W.*, et al.* (2013). Meta-analysis of 74,046 individuals
678 identifies 11 new susceptibility loci for Alzheimer's disease. Nat Genet *45*, 1452-1458.
679 Leek, J.T., Johnson, W.E., Parker, H.S., Jaffe, A.E., and Storey, J.D. (2012). The sva package for
680 removing batch effects and other unwanted variation in high-throughput experiments.
681 Bioinformatics *28*, 882-883.
682 Levy, S., Sutton, G., Ng, P.C., Feuk, L., Halpern, A.L., Walenz, B.P., Axelrod, N., Huang, J., Kirkness,
683 E.F., Denisov, G.*, et al.* (2007). The diploid genome sequence of an individual human. PLoS Biol *5*,
684 e254.
685 Li, B., and Dewey, C.N. (2011). RSEM: accurate transcript quantification from RNA-Seq data with
686 or without a reference genome. BMC Bioinformatics *12*, 323.

687 Lorenzen, A., Samosh, J., Vandewark, K., Anborgh, P.H., Seah, C., Magalhaes, A.C., Cregan, S.P.,
688 Ferguson, S.S.G., and Pasternak, S.H. (2010). Rapid and Direct Transport of Cell Surface APP to
689 the Lysosome defines a novel selective pathway. Molecular Brain *3*, 11.
690 Mallard, F., Antony, C., Tenza, D., Salamero, J., Goud, B., and Johannes, L. (1998). Direct pathway
691 from early/recycling endosomes to the Golgi apparatus revealed through the study of shiga toxin
692 B-fragment transport. J Cell Biol *143*, 973-990.
693 Manders, E., Verbeek, F., and Aten, J. (1993). Measurement of co-localization of objects in dual-
694 colour confocal images. Journal of microscopy *169*, 375-382.
695 Marsh, E.W., Leopold, P.L., Jones, N.L., and Maxfield, F.R. (1995). Oligomerized transferrin
696 receptors are selectively retained by a lumenal sorting signal in a long-lived endocytic recycling
697 compartment. J Cell Biol *129*, 1509-1522.
698 Martin-Belmonte, A., Aguado, C., Alfaro-Ruiz, R., Itakura, M., Moreno-Martinez, A.E., de la Ossa,
699 L., Molnar, E., Fukazawa, Y., and Lujan, R. (2020). Age-Dependent Shift of AMPA Receptors From
700 Synapses to Intracellular Compartments in Alzheimer's Disease: Immunocytochemical Analysis of
701 the CA1 Hippocampal Region in APP/PS1 Transgenic Mouse Model. Front Aging Neurosci *12*,
702 577996.
703 Marwaha, R., and Sharma, M. (2017). DQ-Red BSA Trafficking Assay in Cultured Cells to Assess
704 Cargo Delivery to Lysosomes. Bio Protoc *7*.
705 Maxfield, F.R., and McGraw, T.E. (2004). Endocytic recycling. Nature reviews Molecular cell
706 biology *5*, 121-132.
707 Mayle, K.M., Le, A.M., and Kamei, D.T. (2012). The intracellular trafficking pathway of transferrin.
708 Biochim Biophys Acta *1820*, 264-281.
709 McQuin, C., Goodman, A., Chernyshev, V., Kamentsky, L., Cimini, B.A., Karhohs, K.W., Doan, M.,
710 Ding, L., Rafelski, S.M., Thirstrup, D*., et al.* (2018). CellProfiler 3.0: Next-generation image
711 processing for biology. PLOS Biology *16*, e2005970.
712 Offe, K., Dodson, S.E., Shoemaker, J.T., Fritz, J.J., Gearing, M., Levey, A.I., and Lah, J.J. (2006). The
713 lipoprotein receptor LR11 regulates amyloid beta production and amyloid precursor protein
714 traffic in endosomal compartments. The Journal of neuroscience : the official journal of the
715 Society for Neuroscience *26*, 1596-1603.
716 Olav M. Andersen, N.B., Anne M. Landau, Gro Grunnet Pløen, Anne Mette G. Jensen, Giulia
717 Monti, Benedicte Parm Ulhøi, Jens Randel Nyengaard, Kirsten Rosenmay Jacobsen, Margarita
718 Melnikova Jørgensen, Ida E. Holm, Marianne L. Kristensen, Esben Søvsø Szocska Hansen,
719 Charlotte E. Teunissen, Laura Breidenbach, Mathias Droescher, Ying Liu, Hanne Skovsgaard
720 Pedersen, Henrik Callesen, Yonglun Luo, Lars Bolund, David J. Brooks, Christoffer Laustsen, Scott
721 A. Small, Lars F. Mikkelsen, Charlotte B. Sørensen (2021). In vivo evidence that SORL1, encoding
722 the endosomal recycling receptor SORLA, can function as a causal gene in Alzheimer's Disease.
723 bioRxiv *doi: https://doi.org/10.1101/2021.07.13.452149*.
724 Ouellette, S.P., and Carabeo, R.A. (2010). A Functional Slow Recycling Pathway of Transferrin is
725 Required for Growth of Chlamydia. Front Microbiol *1*, 112.
726 Park, M., Penick, E.C., Edwards, J.G., Kauer, J.A., and Ehlers, M.D. (2004). Recycling endosomes
727 supply AMPA receptors for LTP. Science *305*, 1972-1975.
728 Patapoutian, A., and Reichardt, L.F. (2001). Trk receptors: mediators of neurotrophin action. Curr
729 Opin Neurobiol *11*, 272-280.

730 Pietila, M., Sahgal, P., Peuhu, E., Jantti, N.Z., Paatero, I., Narva, E., Al-Akhrass, H., Lilja, J.,
731 Georgiadou, M., Andersen, O.M.*, et al.* (2019). SORLA regulates endosomal trafficking and
732 oncogenic fitness of HER2. Nat Commun *10*, 2340.
733 Qureshi, Y.H., Patel, V.M., Berman, D.E., Kothiya, M.J., Neufeld, J.L., Vardarajan, B., Tang, M.,
734 Reyes-Dumeyer, D., Lantigua, R., Medrano, M.*, et al.* (2018). An Alzheimer's Disease-Linked Loss-
735 of-Function CLN5 Variant Impairs Cathepsin D Maturation, Consistent with a Retromer Trafficking
736 Defect. Mol Cell Biol *38*.
737 Racoosin, E.L., and Swanson, J.A. (1993). Macropinosome maturation and fusion with tubular
738 lysosomes in macrophages. J Cell Biol *121*, 1011-1020.
739 Raghavan, N.S., Brickman, A.M., Andrews, H., Manly, J.J., Schupf, N., Lantigua, R., Wolock, C.J.,
740 Kamalakaran, S., Petrovski, S., Tosto, G.*, et al.* (2018). Whole-exome sequencing in 20,197
741 persons for rare variants in Alzheimer's disease. Ann Clin Transl Neurol *5*, 832-842.
742 Ramilowski, J.A., Goldberg, T., Harshbarger, J., Kloppmann, E., Lizio, M., Satagopam, V.P., Itoh,
743 M., Kawaji, H., Carninci, P., Rost, B.*, et al.* (2015). A draft network of ligand-receptor-mediated
744 multicellular signalling in human. Nat Commun *6*, 7866.
745 Rapaport, D., Lugassy, Y., Sprecher, E., and Horowitz, M. (2010). Loss of SNAP29 Impairs Endocytic
746 Recycling and Cell Motility. PLOS ONE *5*, e9759.
747 Ren, M., Xu, G., Zeng, J., De Lemos-Chiarandini, C., Adesnik, M., and Sabatini, D.D. (1998).
748 Hydrolysis of GTP on rab11 is required for the direct delivery of transferrin from the pericentriolar
749 recycling compartment to the cell surface but not from sorting endosomes. Proc Natl Acad Sci U
750 S A *95*, 6187-6192.
751 Rogaeva, E., Meng, Y., Lee, J.H., Gu, Y., Kawarai, T., Zou, F., Katayama, T., Baldwin, C.T., Cheng,
752 R., Hasegawa, H.*, et al.* (2007a). The neuronal sortilin-related receptor SORL1 is genetically
753 associated with Alzheimer disease. Nat Genet.
754 Rogaeva, E., Meng, Y., Lee, J.H., Gu, Y., Kawarai, T., Zou, F., Katayama, T., Baldwin, C.T., Cheng,
755 R., Hasegawa, H.*, et al.* (2007b). The neuronal sortilin-related receptor SORL1 is genetically
756 associated with Alzheimer disease. Nat Genet *39*, 168-177.
757 Rohe, M., Hartl, D., Fjorback, A.N., Klose, J., and Willnow, T.E. (2013). SORLA-mediated trafficking
758 of TrkB enhances the response of neurons to BDNF. PLoS One *8*, e72164.
759 Scheltens, P., De Strooper, B., Kivipelto, M., Holstege, H., Chetelat, G., Teunissen, C.E., Cummings,
760 J., and van der Flier, W.M. (2021). Alzheimer's disease. Lancet *397*, 1577-1590.
761 Schindelin, J., Arganda-Carreras, I., Frise, E., Kaynig, V., Longair, M., Pietzsch, T., Preibisch, S.,
762 Rueden, C., Saalfeld, S., Schmid, B.*, et al.* (2012). Fiji: an open-source platform for biological-
763 image analysis. Nat Methods *9*, 676-682.
764 Schmidt, V., Sporbert, A., Rohe, M., Reimer, T., Rehm, A., Andersen, O.M., and Willnow, T.E.
765 (2007). SorLA/LR11 regulates processing of amyloid precursor protein via interaction with
766 adaptors GGA and PACS-1. J Biol Chem *282*, 32956-32964.
767 Seaman, M.N. (2004). Cargo-selective endosomal sorting for retrieval to the Golgi requires
768 retromer. J Cell Biol *165*, 111-122.
769 Seaman, M.N. (2012). The retromer complex - endosomal protein recycling and beyond. J Cell Sci
770 *125*, 4693-4702.
771 Selkoe, D.J. (2002). Alzheimer's disease is a synaptic failure. Science *298*, 789-791.

772 Shi, Y., Kirwan, P., Smith, J., Robinson, H.P., and Livesey, F.J. (2012). Human cerebral cortex
773 development from pluripotent stem cells to functional excitatory synapses. Nat Neurosci *15*, 477-
774 486, S471.
775 Simoes, S., Neufeld, J.L., Triana-Baltzer, G., Moughadam, S., Chen, E.I., Kothiya, M., Qureshi, Y.H.,
776 Patel, V., Honig, L.S., Kolb, H.*, et al.* (2020). Tau and other proteins found in Alzheimer's disease
777 spinal fluid are linked to retromer-mediated endosomal traffic in mice and humans. Science
778 translational medicine *12*.
779 Small, S.A., and Gandy, S. (2006). Sorting through the cell biology of Alzheimer's disease:
780 intracellular pathways to pathogenesis. Neuron *52*, 15-31.
781 Small, S.A., and Petsko, G.A. (2020). Endosomal recycling reconciles the Alzheimer's disease
782 paradox. Science translational medicine *12*.
783 Sonnichsen, B., De Renzis, S., Nielsen, E., Rietdorf, J., and Zerial, M. (2000). Distinct membrane
784 domains on endosomes in the recycling pathway visualized by multicolor imaging of Rab4, Rab5,
785 and Rab11. J Cell Biol *149*, 901-914.
786 Spoelgen, R., von Arnim, C.A., Thomas, A.V., Peltan, I.D., Koker, M., Deng, A., Irizarry, M.C.,
787 Andersen, O.M., Willnow, T.E., and Hyman, B.T. (2006). Interaction of the cytosolic domains of
788 sorLA/LR11 with the amyloid precursor protein (APP) and beta-secretase beta-site APP-cleaving
789 enzyme. The Journal of neuroscience : the official journal of the Society for Neuroscience *26*, 418-
790 428.
791 Sun, J., and Roy, S. (2018). The physical approximation of APP and BACE-1: A key event in
792 alzheimer's disease pathogenesis. Dev Neurobiol *78*, 340-347.
793 Temkin, P., Morishita, W., Goswami, D., Arendt, K., Chen, L., and Malenka, R. (2017). The
794 Retromer Supports AMPA Receptor Trafficking During LTP. Neuron *94*, 74-82 e75.
795 Thonberg, H., Chiang, H.H., Lilius, L., Forsell, C., Lindstrom, A.K., Johansson, C., Bjorkstrom, J.,
796 Thordardottir, S., Sleegers, K., Van Broeckhoven, C.*, et al.* (2017). Identification and description
797 of three families with familial Alzheimer disease that segregate variants in the SORL1 gene. Acta
798 Neuropathol Commun *5*, 43.
799 Wakabayashi, K., Narisawa-Saito, M., Iwakura, Y., Arai, T., Ikeda, K., Takahashi, H., and Nawa, H.
800 (1999). Phenotypic down-regulation of glutamate receptor subunit GluR1 in Alzheimer's disease.
801 Neurobiol Aging *20*, 287-295.
802 Wang, Y., Eng, D.G., Kaverina, N.V., Loretz, C.J., Koirala, A., Akilesh, S., Pippin, J.W., and
803 Shankland, S.J. (2020). Global transcriptomic changes occur in aged mouse podocytes. Kidney Int
804 *98*, 1160-1173.
805 Willnow, T.E., and Andersen, O.M. (2013). Sorting receptor SORLA--a trafficking path to avoid
806 Alzheimer disease. J Cell Sci *126*, 2751-2760.
807 Yap, C.C., Digilio, L., McMahon, L.P., Garcia, A.D.R., and Winckler, B. (2018). Degradation of
808 dendritic cargos requires Rab7-dependent transport to somatic lysosomes. Journal of Cell Biology
809 *217*, 3141-3159.
810 Yasuda, R.P., Ikonomovic, M.D., Sheffield, R., Rubin, R.T., Wolfe, B.B., and Armstrong, D.M.
811 (1995). Reduction of AMPA-selective glutamate receptor subunits in the entorhinal cortex of
812 patients with Alzheimer's disease pathology: a biochemical study. Brain Res *678*, 161-167.
813 Young, J.E., Boulanger-Weill, J., Williams, D.A., Woodruff, G., Buen, F., Revilla, A.C., Herrera, C.,
814 Israel, M.A., Yuan, S.H., Edland, S.D.*, et al.* (2015). Elucidating Molecular Phenotypes Caused by

815 the SORL1 Alzheimer's Disease Genetic Risk Factor Using Human Induced Pluripotent Stem Cells.
816 Cell stem cell *16*, 373-385.
817 Yuan, S.H., Martin, J., Elia, J., Flippin, J., Paramban, R.I., Hefferan, M.P., Vidal, J.G., Mu, Y., Killian,
818 R.L., Israel, M.A.*, et al.* (2011). Cell-surface marker signatures for the isolation of neural stem
819 cells, glia and neurons derived from human pluripotent stem cells. PLoS One *6*, e17540.
820 Zigdon, H., Meshcheriakova, A., Farfel-Becker, T., Volpert, G., Sabanay, H., and Futerman, A.H.
821 (2017). Altered lysosome distribution is an early neuropathological event in neurological forms
822 of Gaucher disease. FEBS Lett *591*, 774-783.
823

Figure legends

Figure 1. Loss of *SORL1* expression leads to increased TRKB and GLUA1 localization in early endosomes. Representative immunofluorescent images of WT and *SORL1*KO neurons showing increased colocalization of **(a)** TRKB (green) and **(b)** GLUA1 (green) with EEA1 (red). All neurons were immunolabeled with MAP2 (far-red) and counterstained with DAPI (blue). Scale bar: 10μm. In all cases, quantification of colocalization was represented as Mander's correlation co-efficient (MCC). 10-20 images were analyzed per genotype. Two isogenic clones of each genotype were used in all experiments. Data represented as mean ± SD. Normally distributed data was analyzed using parametric two-tailed unpaired t test and non-normally distributed data was analyzed by non-parametric Mann Whitney test. Significance was defined as a value of *$p < 0.05$, **$p < 0.01$, ***$p < 0.001$, and ****$p < 0.0001$.

Figure 2. Loss of *SORL1* expression impairs trafficking to late endosomes and lysosomes.

a) *SORL1*KO neurons show reduced lysosomal proteolytic activity as measured by DQ Red BSA. Representative immunofluorescent images of WT and *SORL1*KO neurons showing double immunolabeling for MAP2 (green) and DQ Red BSA (red). Scale bar: 10μm Quantification of fluorescence intensity of DQ Red BSA using ImageJ software. **(b-f)** *SORL1*KO neurons show reduced colocalization of cargo with late endosomes and lysosomes. Representative immunofluorescent images of WT and *SORL1*KO neurons showing reduced colocalization of **(b)** TRKB (green) and **(c)** GLUA1 (green) with Rab7 positive late endosomes (red) in *SORL1*KO neurons. Representative immunofluorescent images of WT and *SORL1*KO neurons showing reduced colocalization of **(d)** APP (green) and **(e)** TRKB (green) and **(f)** GLUA1 (green) with LAMP1 positive lysosomes (red) in *SORL1*KO neurons. Scale bar: 10μm. In all cases, quantification of colocalization was represented as Mander's correlation co-efficient (MCC). 10-20 images were analyzed per genotype. Two isogenic clones of each genotype were used in all experiments. Data represented as mean ± SD. Normally distributed data was analyzed using parametric

two-tailed unpaired t test and non-normally distributed data was analyzed by non-parametric Mann Whitney test. Significance was defined as a value of *p < 0.05, **p < 0.01, ***p < 0.001, and ****p < 0.0001.

Figure 3. Loss of *SORL1* impacts the cell surface recycling pathway

a) *SORL1*KO neurons show slower rate of transferrin recycling. Quantification of fluorescence intensity of intracellular transferrin at different time points after treating cells with Alexa Fluor 647-conjugated transferrin for 15 mins, using ImageJ software. Data represented as percent of time 0 fluorescence intensity. **(b)** *SORL1*KO neurons show larger recycling endosomes. Representative immunofluorescent images of WT and *SORL1*KO neurons labeled with antibodies for MAP2 (red) and Rab11 (green). Nuclei were counterstained with DAPI (blue). Scale bar: 5μm. Quantification of size of Rab11 labeled recycling endosomes using CellProfiler software. Representative immunofluorescent images of WT and *SORL1*KO neurons showing increased colocalization of **(c)** APP (green), **(d)** TRKB (green) and **(e)** GLUA1 (green) with Rab11 positive recycling endosomes (red) in *SORL1*KO neurons. Scale bar:10mm In all cases, quantification of colocalization was represented as Mander's correlation co-efficient (MCC). 10-20 images were analyzed per genotype. Two isogenic clones of each genotype were used in all experiments. Data represented as mean ± SD. Normally distributed data was analyzed using parametric two-tailed unpaired t test and non-normally distributed data was analyzed by non-parametric Mann Whitney test. Significance was defined as a value of *p < 0.05, **p < 0.01, ***p < 0.001, and ****p < 0.0001.

Figure 4. Loss of *SORL1* expression impairs recycling to the cell surface.

a-b) *SORL1*KO neurons show reduced cell surface expression of APP **(a)** and GLUA1 **(b)**. Representative immunofluorescent images of WT and *SORL1*KO neurons labeled with antibodies for APP **(a)** (red) and GLUA1 **(b)** (red). Scale bar: 5μm. Intensity of APP and GLUA1 measured using ImageJ software. Data is presented as a ratio of surface intensity to total intensity. Two isogenic clones of each genotype were used in all experiments.

Data represented as mean ± SD. Normally distributed data was analyzed using parametric two-tailed unpaired t test. Significance was defined as a value of *p < 0.05, **p < 0.01, ***p < 0.001, and ****p < 0.0001.

Figure 5. Overexpression of *SORL1* enhances endosomal recycling.

a) *SORL1*OE neurons show faster rate of transferrin recycling. Quantification of fluorescence intensity of intracellular transferrin at different time points after treating cells with Alexa Fluor 647-conjugated transferrin for 15 mins, using ImageJ software. Data represented as percent of time 0 fluorescence intensity. **(b)** *SORL1*OE neurons show reduced size of recycling endosomes. Representative immunofluorescent images of WT and *SORL1*OE neurons labeled with Rab11 (green) and MAP2 (red) showing smaller Rab11 positive recycling endosomes in *SORL1*OE neurons. Nuclei counterstained with DAPI (blue). Quantification of Rab11+ recycling endosome size performed using Cell Profiler software and represented as area of Rab11+ vesicles. Scale bar: 5μm. Representative immunofluorescent images of WT and *SORL1*OE neurons showing increased colocalization of **(c)** APP (green), **(d)** TRKB (green) and **(e)** GLUA1 (green) with Rab11 (red) positive recycling endosomes. *SORL1*OE neurons and controls have endogenous GFP expression due to the piggybac vector system. GFP fluorescence is pseudo-colored (Far-red) and was used to outline cell bodies. Quantification of colocalization with Rab11 represented as Mander's Correlation Co-efficient (MCC). Scale bar: 10μm. Representative immunofluorescent images of WT and *SORL1*OE neurons showing increased cell surface expression of **(f)** APP (red) and **(g)** GLUA1 (red) in *SORL1*OE neurons. Scale bar: 5μm Fluorescence intensity of APP and GLUA1 measured using ImageJ software. Data is presented as a ratio of surface intensity to total intensity. Nuclei counterstained with DAPI. Two isogenic clones of each genotype were used in all experiments. Data represented as mean ± SD. Normally distributed data was analyzed using parametric two-tailed unpaired t test. Significance defined as a value of *p < 0.05, **p < 0.01, ***p < 0.001, and ****p < 0.0001.

Figure 6. Analysis of bulk RNA-sequencing data indicates alterations in cell surface and extracellular trafficking, receptor-ligand and channel activity.

Gene ontology analysis of DEGs in WT and *SORL1*KO neurons. Shown here are the top upregulated **(a)** and downregulated **(b)** molecular function terms in *SORL1*KO neurons. GO annotation terms are listed on the y-axis, adjusted p-value is shown on the x-axis. **(c)** Ligand-receptor network changes in *SORL1*KO neurons, identified if genes are more than 1.5-fold increased or decreased in *SORL1*KO neurons with an adjusted p-value less than 0.05. Circles denote ligands, squares denote receptors, blue indicates genes expressed significantly lower in *SORL1*KO neurons, red indicates genes expressed significantly higher in *SORL1*KO neurons. Arrows point from ligand to receptor, denoting receptor-ligand interactions. Black arrows denote consistent expression changes between ligand and receptor, indicating that both genes in the pair are either upregulated or downregulated. Gray arrows denote inconsistent changes between ligand and receptor. Clusters impacted by cell surface recycling (β-integrins, ephrins) or neurotrophic signaling (FGF/FGFR, NGF/NGFR) are indicated by green dotted arrows.

Supplementary figures

Supplementary figure 1

a) *SORL1*KO neurons show larger lysosome size and increased lysosome number. Representative immunofluorescent images of WT and *SORL1*KO neurons labeled with LAMP1 (green) and MAP2 (red) showing increased LAMP1 positive vesicle size in *SORL1*KO neurons. Quantification of LAMP1 size and number was performed using Cell Profiler software. LAMP1 size is represented as area of LAMP1 positive vesicles, and LAMP1 number is represented as number of LAMP1 positive vesicles per square micron of cell area. Scale bar: 5μm **(b)** *SORL1*KO neurons show no change in colocalization of lysosomes with the lysosomal enzyme Cathepsin D. Representative immunofluorescent images of WT and *SORL1*KO neurons labeled with antibodies for LAMP1 (green), Cathepsin D (red) and MAP2 (Far-red) showing no alteration in colocalization of Cathepsin-D with LAMP1 in *SORL1*KO neurons. Nuclei counterstained with DAPI (blue). Scale bar: 10μm Quantification of colocalization of LAMP1 with Cathepsin-D represented as Mander's correlation coefficient (MCC). 10-20 images

were analyzed per genotype. Two isogenic clones of each genotype were used in all experiments. Data represented as mean ± SD. Significance was determined using two-tailed unpaired Student's t-test and defined as a value of *p < 0.05, **p < 0.01, ***p < 0.001, and ****p < 0.0001.

Supplemental figure 2

a) *SORL1*OE neurons show no change in lysosomal proteolytic activity as measured using DQ Red BSA. Representative immunofluorescent images of WT and *SORL1*OE neurons showing double immunolabeling for MAP2 (green) and DQ Red BSA (red). Scale bar: 10μm. Quantification of fluorescence intensity of DQ Red BSA using ImageJ software. Representative immunofluorescent images of WT and *SORL1*OE neurons showing increased colocalization of APP, TRKB and GLUA1 (green) with Rab7 (red) **(b-d)** and LAMP1 (red) **(e-g)** in *SORL1*OE neurons. *SORL1*OE neurons and controls have endogenous GFP expression due to the piggybac vector system. GFP fluorescence is pseudo-colored (Far-red) and was used to outline cell bodies. Scale bar: 10μm. Nuclei are counterstained with DAPI (blue). In all cases, quantification of colocalization was represented as Mander's correlation co-efficient (MCC). 10-20 images were analyzed per genotype. Two isogenic clones of each genotype were used in all experiments. Data represented as mean ± SD. Significance was determined using two-tailed unpaired Student's t-test and was defined as a value of *p < 0.05, **p < 0.01, ***p < 0.001, and ****p < 0.0001.

Supplemental figure 3

a) Principle component analysis (PCA) plot of all RNAseq samples using all expressed genes. Samples are color coded by differentiation batch. Triangles represent WT samples, circles represent *SORL1*KO. Genotype accounts for the highest variance (37%, PC1, x-axis). **b)** Volcano plot. Log2 fold change between *SORL1*KO and WT is shown along the x-axis. Statistical significance is shown along the y-axis, and is measured by adjusted p-value. Genes upregulated in *SORL1*KO neurons are shown by red circles, genes downregulated in *SORL1*KO neurons are shown by blue circles. We observed 6643 DEGs, with 2819 upregulated and 3824 downregulated.

There are significantly more down regulated genes than upregulated genes ($p<2.2e-16$). Grey circles represent genes that are not significantly differentially expressed.

Figure 1

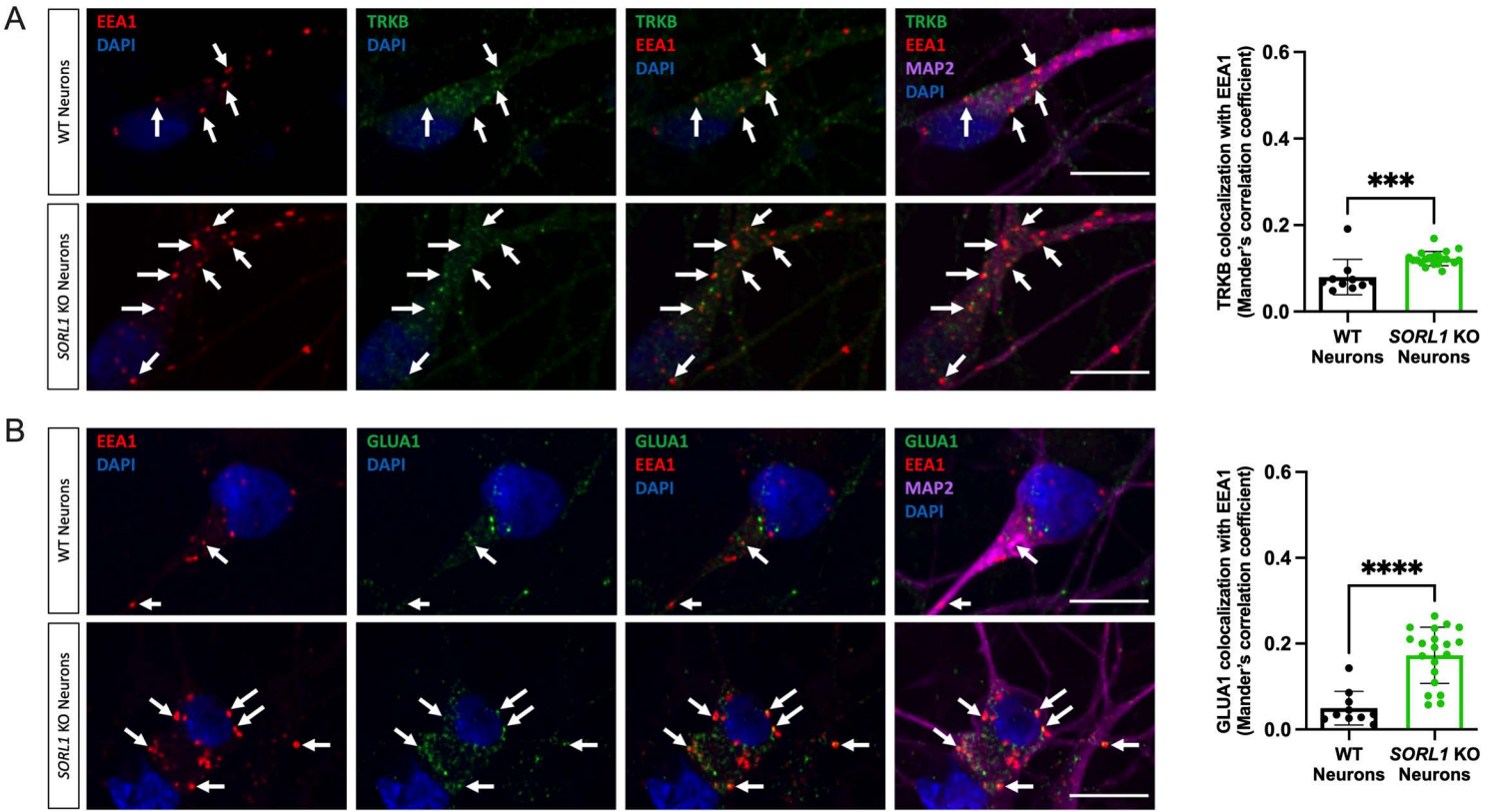
A
WT Neurons
SORL1 KO Neurons
EEA1
DAPI
TRKB
DAPI
TRKB
EEA1
DAPI
TRKB
EEA1
MAP2
DAPI
TRKB colocalization with EEA1
(Mander's correlation coefficient)
0.6
0.4
0.2
0.0
***
WT Neurons
SORL1 KO Neurons
B
WT Neurons
SORL1 KO Neurons
EEA1
DAPI
GLUA1
DAPI
GLUA1
EEA1
DAPI
GLUA1
EEA1
MAP2
DAPI
GLUA1 colocalization with EEA1
(Mander's correlation coefficient)
0.6
0.4
0.2
0.0
****
WT Neurons
SORL1 KO Neurons

Figure 2

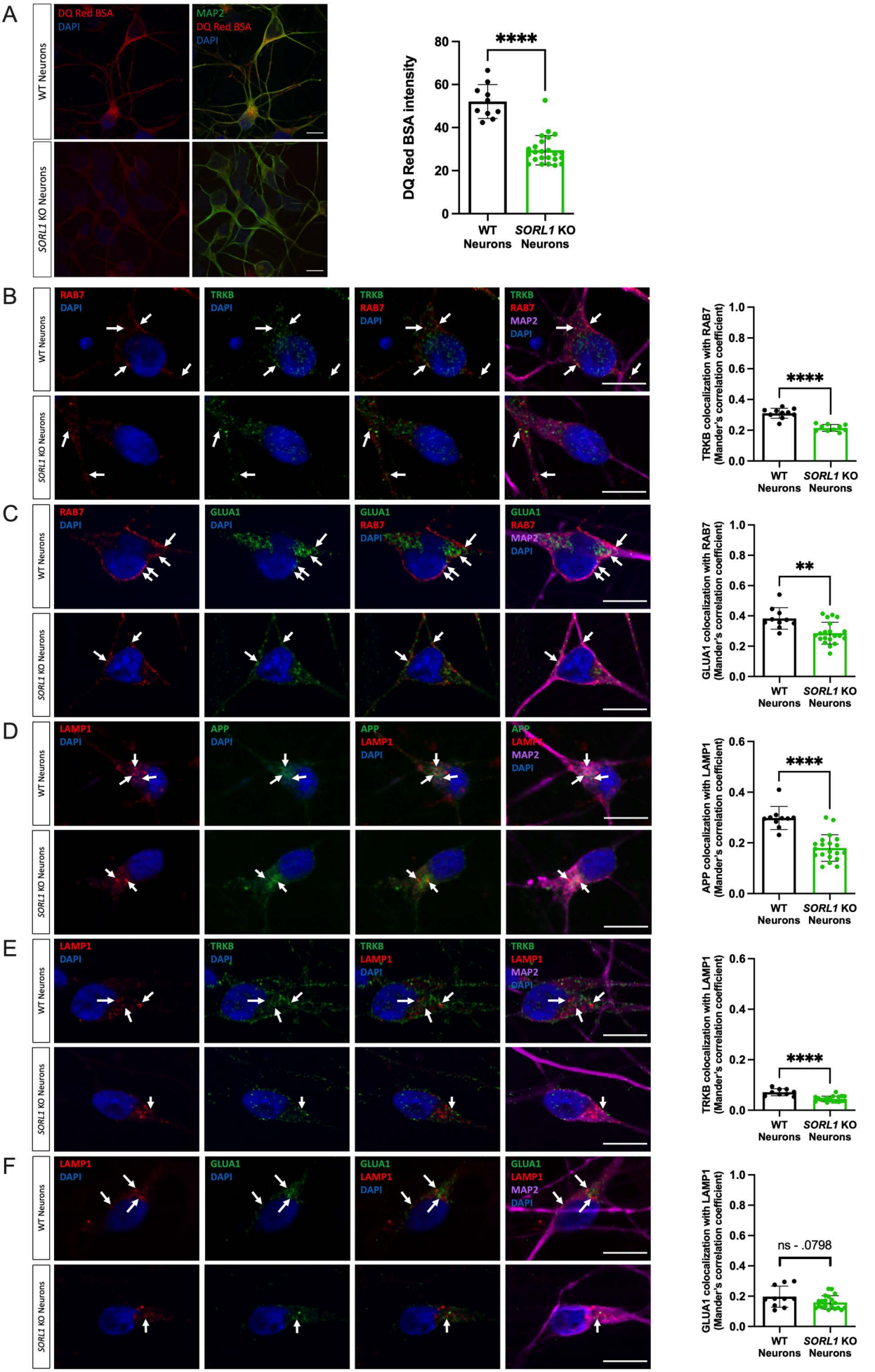
A
WT Neurons
SORL1 KO Neurons
DQ Red BSA
DAPI
MAP2
DQ Red BSA intensity
****
WT Neurons
SORL1 KO Neurons
B
RAB7
TRKB
MAP2
TRKB colocalization with RAB7 (Mander's correlation coefficient)
C
GLUA1
GLUA1 colocalization with RAB7 (Mander's correlation coefficient)
**
D
LAMP1
APP
APP colocalization with LAMP1 (Mander's correlation coefficient)
E
TRKB colocalization with LAMP1 (Mander's correlation coefficient)
F
GLUA1 colocalization with LAMP1 (Mander's correlation coefficient)
ns - .0798

Figure 3

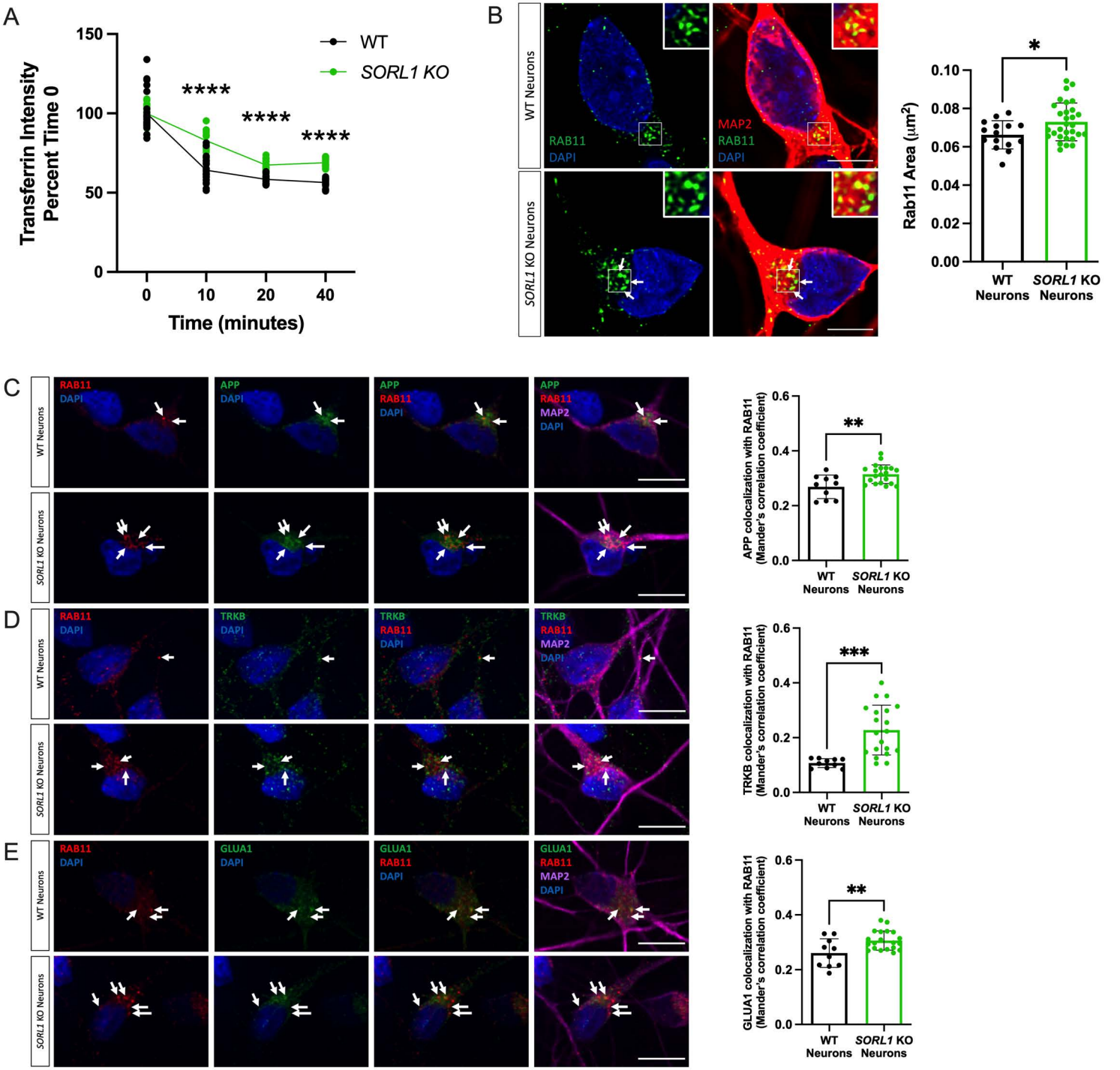
A
Transferrin Intensity Percent Time 0
Time (minutes)
WT
SORL1 KO
****
B
WT Neurons
SORL1 KO Neurons
RAB11
DAPI
MAP2
Rab11 Area (μm²)
C
APP
D
TRKB
E
GLUA1
APP colocalization with RAB11 (Mander's correlation coefficient)
TRKB colocalization with RAB11 (Mander's correlation coefficient)
GLUA1 colocalization with RAB11 (Mander's correlation coefficient)

Figure 4

A

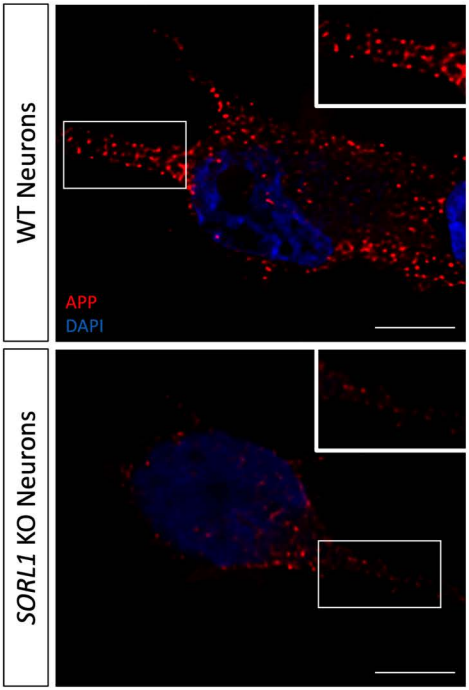
WT Neurons
APP
DAPI
SORL1 KO Neurons

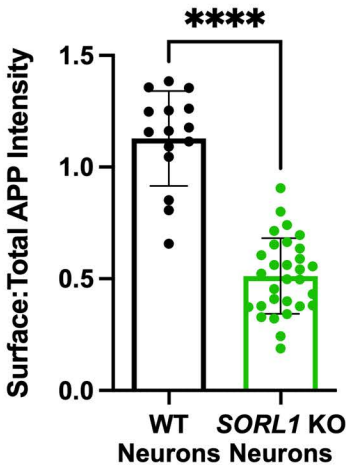
****
Surface:Total APP Intensity
1.5
1.0
0.5
0.0
WT Neurons
SORL1 KO Neurons

B

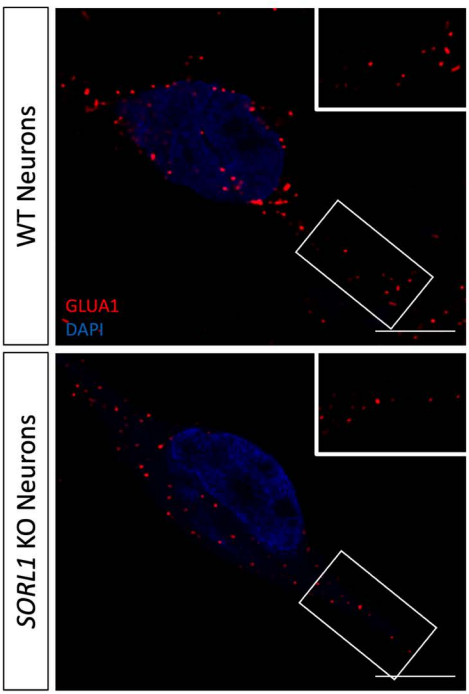
WT Neurons
GLUA1
DAPI
SORL1 KO Neurons

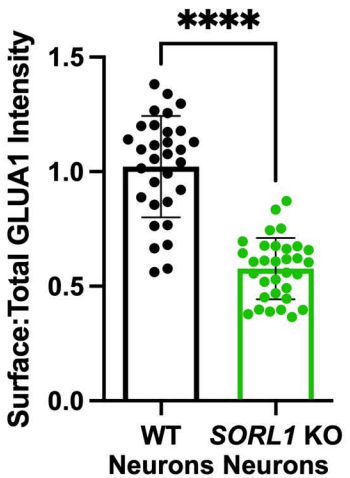
****
Surface:Total GLUA1 Intensity
1.5
1.0
0.5
0.0
WT Neurons
SORL1 KO Neurons

Figure 5

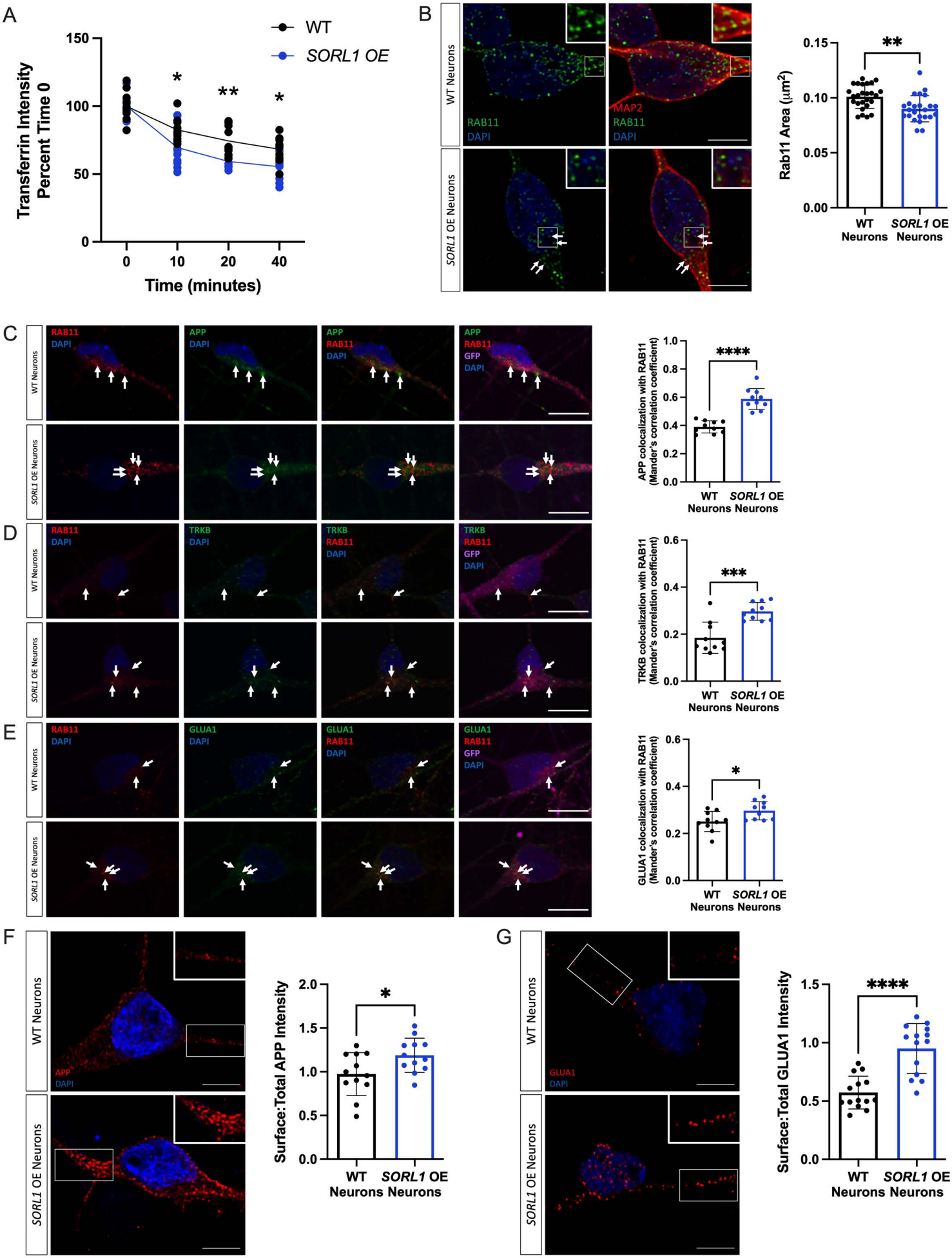
A
WT
SORL1 OE
Transferrin Intensity Percent Time 0
Time (minutes)
B
WT Neurons
SORL1 OE Neurons
RAB11
DAPI
MAP2
Rab11 Area (μm²)
C
APP
GFP
APP colocalization with RAB11 (Mander's correlation coefficient)
D
TRKB
TRKB colocalization with RAB11 (Mander's correlation coefficient)
E
GLUA1
GLUA1 colocalization with RAB11 (Mander's correlation coefficient)
F
Surface:Total APP Intensity
G
Surface:Total GLUA1 Intensity

Figure 6

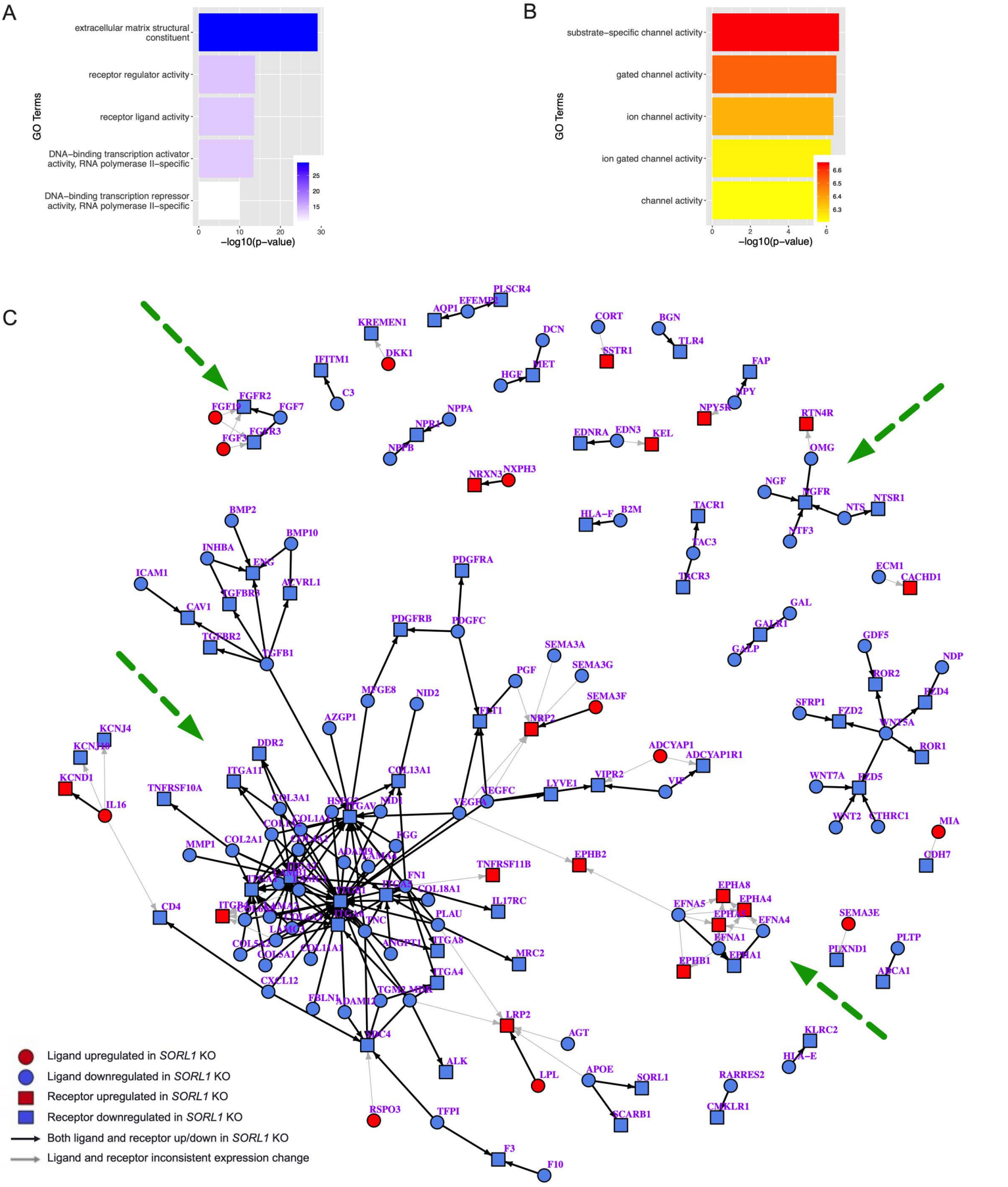
A
extracellular matrix structural constituent
receptor regulator activity
receptor ligand activity
DNA−binding transcription activator activity, RNA polymerase II−specific
DNA−binding transcription repressor activity, RNA polymerase II−specific
GO Terms
−log10(p−value)
B
substrate−specific channel activity
gated channel activity
ion channel activity
ion gated channel activity
channel activity
GO Terms
−log10(p−value)
C
Ligand upregulated in SORL1 KO
Ligand downregulated in SORL1 KO
Receptor upregulated in SORL1 KO
Receptor downregulated in SORL1 KO
Both ligand and receptor up/down in SORL1 KO
Ligand and receptor inconsistent expression change